JOURNAL OF GEOPHYSICAL RESEARCH, VOL. 106, NO. B6, PAGES 10,941–10,960, JUNE 10, 2001

A geomagnetic record over the last 3.5 million years from deep-tow magnetic anomaly profiles across the Central Indian Ridge

Gaud Pouliquen, Yves Gallet, and Philippe Patriat
UMR 7577, Institut de Physique du Globe de Paris, Paris, France

Jérôme Dyment
UMR 6538, Institut Universitaire Européen de la Mer, Université de Bretagne Occidentale, Plouzané, France

Chiori Tamura
Ocean Research Institute, University of Tokyo, Tokyo, Japan

Abstract. High-resolution records of the geomagnetic field intensity over the last 4 Myr provided by paleomagnetic analyses of marine sediments have shown the occurrence of short-lived low field intensity features associated with excursions or short polarity intervals. In order to evaluate the ability of marine magnetic anomalies to record the same geomagnetic events, we have collected six deep-tow (~500 m above the seafloor) and several sea surface magnetic anomaly profiles from the Central Indian Ridge across the Brunhes, Matuyama, and Gauss chrons (i.e., from the ridge axis to anomaly 2A). After removal of topography, latitude, and azimuth effects, we converted distances into time sequences using well-dated polarity reversal anomalies as tie points. We calculated the average signal to test the robustness of the short-wavelength anomalies. The resulting stacked profile is very similar to stacked sea surface and downward continued profiles from the Central Indian Ridge, the East Pacific Rise, and the Pacific-Antarctic Ridge. Our results suggest that in addition to polarity reversals, to previously suggested geomagnetic events (subchrons or excursions) within the Brunhes and Matuyama chrons. A new small-scale magnetic anomaly, likely generated by several closely spaced geomagnetic field intensity variations represent the major contributor to the detailed shape of recent marine magnetic anomalies in investigated areas. We observe a dense succession of microanomalies that are correlated excursions (Ontong Java 1 and 2, and Gilsa), is found after the Olduvai chron. The near-bottom results support the existence of three geomagnetic features between the Gauss-Matuyama boundary and Olduvai. They also suggest three geomagnetic events during the C2A.1n subchron within the Gauss chron. This study emphasizes the potential of deep-tow magnetic surveys in detecting fluctuations in geomagnetic field intensity and, in particular, short-lived excursions, a poorly constrained part of the geomagnetic field temporal variation spectrum.

1. Introduction

The detailed chronology of geomagnetic field reversals during the Mesozoic and the Cenozoic was largely established from magnetic anomaly profiles obtained from different oceanic basins, together with numerous magnetostratigraphic, biostratigraphic and radiometric studies [*Cande and Kent*, 1992a; *Harland et al.*, 1989]. Because these oceanic magnetic anomaly profiles were acquired at sea level, relatively far from the magnetic sources, the geomagnetic polarity timescale is known with a limited resolution of ~30-50 kyr. In an attempt to increase this resolution, *Blakely and Cox* [1972] and *Blakely* [1974] used a stacking technique which revealed short-wavelength magnetic anomalies, called "tiny wiggles," in addition to the well-known reversal pattern [*LaBrecque et al.*, 1977; *Cande and Kent*, 1992a,1992b].

The origin of the short-wavelength magnetic anomalies has been highly debated and nonexclusive interpretations have been proposed. First, the existence of tiny wiggles could reflect the complexity of the crustal formation process [e.g., *Klitgord et al.*, 1975; *Tivey and Jonhson*, 1987, 1993] and/or varying magnetic properties of the extrusive basalt layer [e.g., *Gee and Kent*, 1994]. The correlation of tiny wiggles sequences from distant areas (e.g., within the C12r and C24r [*Cande and Kent*, 1992b]) supports a second alternative for which the small-scale anomalies would be related to geomagnetic field behavior [*Cande and Kent*, 1992b; *Gee et al.*, 1996; *Lanci and Lowrie*, 1997]. In this case, these anomalies could reflect either large fluctuations of the geomagnetic field intensity or very short magnetic polarity intervals (subchrons). Furthermore, recent magnetostratigraphic studies of marine sediments show that the geomagnetic field experienced large and

Paper number 2000JB900442.
0148-0227/01/2000JB90044$09.00

rapid changes in intensity through the last 4 Myr, with several short periods of low intensity likely related to excursional events and not to reversals [e.g., *Valet and Meynadier*, 1993; *Guyodo and Valet*, 1999]. Within the Brunhes chron, up to 14 such events have been proposed [e.g., *Champion et al.*, 1988; *Langereis et al.*, 1997; *Guyodo and Valet*, 1999], and Gubbins [1999] underlined the importance of their detection for characterizing the geomagnetic field behavior.

In order to test whether the oceanic crust records geomagnetic field paleointensity variations, *Gee et al.* [1996] compared synthetic anomaly models constructed from the paleointensity sedimentary records proposed by *Valet and Meynadier* [1993] and *Guyodo and Valet* [1996] for the last 800 kyr with sea surface magnetic anomaly profiles at various spreading rates. They found evidence that marine magnetic anomalies indeed strongly reflect paleointensity fluctuations. More recently, *Schouten et al.* [1999] argued that both field- and accretion-related sources shape the oceanic magnetic anomalies near the ridge crest.

To further test the possibility that oceanic magnetic anomaly profiles resolve geomagnetic field intensities, we decided to compare high-resolution (i.e., near-bottom) anomaly profiles, which give a more detailed picture of the anomalies [*Macdonald*, 1977; *Perram et al.*, 1990], with the paleointensity data available for the last few million years. In this paper, we present an analysis of three deep-tow oceanic magnetic profiles acquired on the Central Indian Ridge (CIR) over the Brunhes, Matuyama, and Gauss chrons. This analysis is extended to sea surface anomaly profiles from the CIR, the East Pacific Rise (EPR), and the Pacific-Antarctic Ridge (PAR). A consistent pattern of microanomalies is obtained. These microanomalies can be correlated to one or several geomagnetic events, each marked by a pronounced low field intensity.

2. Data Acquisition and Processing

2.1. Regional Setting and Data Acquisition

As part of the Magofond 2 cruise (October-November 1998), R/V *Marion Dufresne* surveyed the Central Indian Ridge between 18.5°S and 20°S [*Dyment et al.*, 1999a]. This area was selected for its moderate topographic roughness and for its regular abyssal hills pattern (Figure 1). The absence of a well-developed segmentation along the CIR at the survey area suggests that despite a relatively slow spreading rate (average full rate of ~43 km/Myr), the area bears similarities to intermediate to fast spreading centers. This may indicate a rather simple magnetic source, undisturbed by three-dimensional architecture effects [*Dyment and Arkani-Hamed*, 1995]. The moderate spreading rate of the CIR yields a limited time resolution compared to the one we could have obtained from faster spreading ridge system, but on the other hand, this rate offers the possibility to record magnetic profiles with a relatively large time coverage. Each profile provides two conjugate records of the same time interval on both sides of the spreading center, enabling us to separate true geomagnetic signal from anomalies associated with crustal emplacement and tectonic processes (such as small ridge jumps or ridge propagation).

Three deep-tow magnetic profiles were collected from the axis to the Gauss chron inclusive (anomaly 2A; up to ~3.5 Ma). Along these profiles (A, B, C; Figure 1), the total magnetic field was measured with a Deep-Towed Proton magnetometer (DTPM) provided by the Ocean Research Institute of Tokyo. This equipment, described by *Sayanagi et al.* [1994], is a self-contained system which also contains a depth meter. Each near-bottom profile was acquired in a single continuous transect at an average speed of ~2.5 knots. In order to integrate a roughly constant source thickness, the instrument was towed as much as possible at a constant distance from the seafloor (~500 m from the bottom), which was made possible by controlling the ship speed and the wire length (Figure 2). A second depth meter installed ahead of the depressing weight and connected to the ship through a conducting cable was used to monitor the DTPM altitude. During deep-tow experiments the magnetic field was also measured at sea surface using a standard proton magnetometer (profiles sA, sB, and sC; Figure 1). In addition, 11 other sea surface magnetic profiles were acquired between 20.2°S/65.5°E and 18.6°S/66°E, providing a regional coverage of the geomagnetic field (s18 to s35; Figure 1).

2.2. Near-Bottom Data Processing

Measurements were carried out every 1 min yielding a spatial sampling interval of ~80 m. The magnetic data were resampled to an even interval of 200 m. We used the cable length record to merge the magnetic data with the ship position as no transponder was attached to the deep-towed magnetometer. The magnetic data were corrected for the regional geomagnetic field determined from the 1995 International Geomagnetic Reference Field (IGRF) calculated at each measurement location [*International Association of Geomagnetism and Aeronomy*, 1996]. The total field anomaly profiles were first upward continued using the Fourier-based method of *Guspi* [1987] to a level plane at 2000 m below sea level. We acknowledge that the high-cut filtering and the upward continuation process induce a loss in resolution, mainly for the deepest (and older) parts of the profiles, and for those of high topographic contrast (i.e., in the axial valley [Hussenoeder et al., 1995]). However, the comparison between the data before and after reduction shows that this resolution loss only affects very short wavelengths (<1.2 km, i.e., ~50 kyr), and it is obviously of minor importance. The latitude and azimuth dependence of the magnetic anomaly profiles was removed using the "theta method" of *Schouten and McCamy* [1972]. In the investigated area the geocentric dipole direction is D=-18°, I=-52°, and the calculated skewness is 44°. Using the *Parker and Huestis* [1974] method, we inverted the magnetic anomaly profiles to equivalent magnetization distributions assuming a 500-m-thick source layer. Convergence toward a solution was ensured with a band-passed filter with a short-wavelength cutoff, cosine-tapered between 2.4 and 1.2 km. For each profile, we used a two-dimensional Fourier-based forward method [*Parker*, 1973] to compute a topography-corrected magnetic anomaly profile at 2500 m below sea level [*Ravilly et al.*, 1998].

2.3. Sea Surface Magnetic Profiles

The profiles were resampled at intervals of 0.5 km and reduced to the pole (latitude and azimuth corrected, i.e., deskewed) using the same parameters as for the deep-tow profiles. The simultaneous acquisition of deep-tow and sea surface anomaly profiles had two principal objectives. The

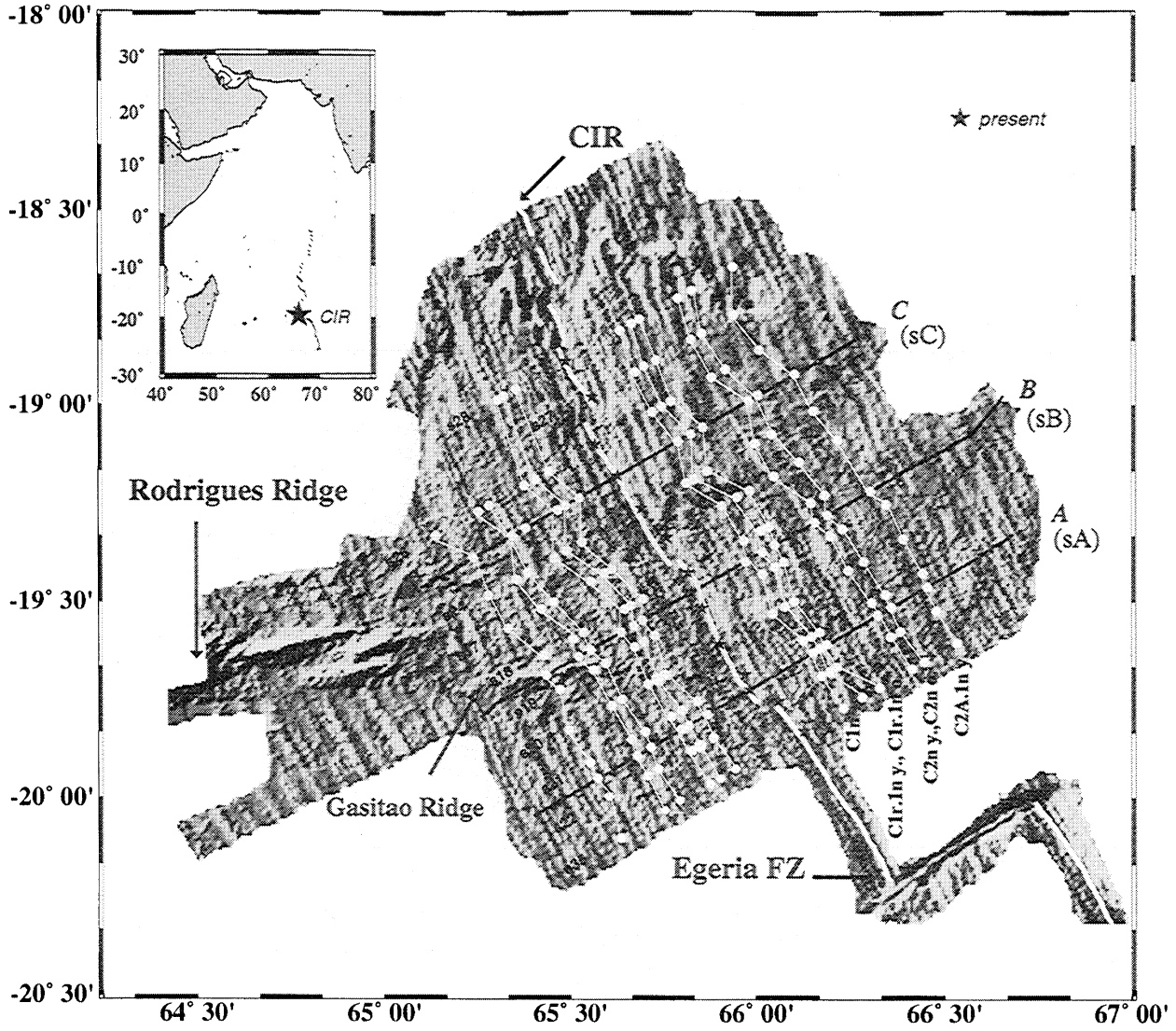

Figure 1. Shaded multibeam bathymetry of the survey area on the CIR with a N300° illumination (500 m gridding). The stars show the magnetic axis and the white line shows the bathymetric axis. Black lines indicate the deep-tow track lines (A, B, C) and their correspondent sea surface profiles (sA, sB, sC). The picked anomalies identified along the downward continued sea surface profiles and shown by dots are referenced following the *Cande and Kent* [1995] nomenclature.

first was to test whether the major contribution to the magnetic signal is indeed provided by the extrusive basaltic layer [*Schouten and Denham*, 1979; *Tivey and Johnson,* 1993; *Cande and Kent*, 1976]. For this, the equivalent magnetization distribution was computed for the three sea surface profiles using the two-dimensional (2-D) method of *Parker and Huestis* [1974], again assuming a 500-m source thickness. The annihilator, i.e., the magnetization producing no external magnetic field, was chosen as the difference between a constant magnetization distribution (e.g., 1 A/m) and the inversion computed from the forward calculation of this distribution. The topography-corrected magnetic anomaly profiles were computed at an observation plane 2000 m below sea level (and a 2500-m-deep magnetization distribution with a flat topography). The good agreement observed in Figure 3 between the topography-corrected deep-tow and downward continued sea surface profiles strongly suggests that in the investigated CIR area the primary sources of the detailed shape of the anomalies are shallow, likely in the extrusive basaltic layer. This indicates that other downward continued sea surface anomaly profiles can be used to extend the high-resolution magnetic data on a regional scale and therefore to test the robustness of the short-wavelength anomalies observed in deep-tow data. Inversion of the sea level magnetic profiles was performed using a band-pass filter, for which the short wavelength cutoff of 2.2 km, cosine-tapered between 4.4 and 2.2 km, was adjusted to obtain the best fit between the three deep-tow anomaly profiles and the corresponding downward continued sea surface anomaly profiles.

3. Identification of the Magnetic Polarity Intervals

3.1. Picking the Principal Reversal Boundaries on Surface Anomaly Profiles

Major geomagnetic reversal boundaries (i.e., Brunhes-Matuyama, Jaramillo and Olduvai young and old boundaries,

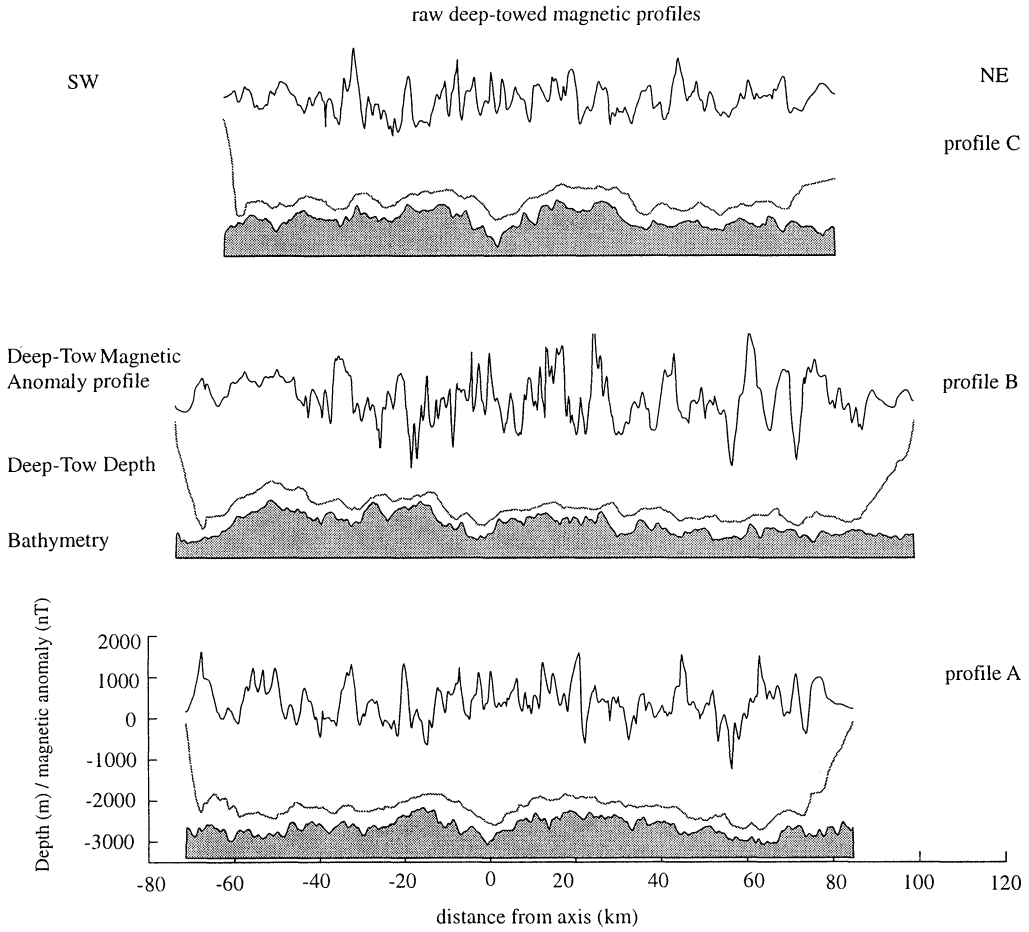

Figure 2. Near-bottom magnetic data corrected from the IGRF 1995 regional gradient and deep-towed proton magnetometer altitude for the three deep-tow profiles. Seafloor topography is shaded.

and Matuyama-Gauss boundary) were identified on downward continued sea surface profiles (Figure 4). The same boundaries were picked on the deep-tow magnetic profiles, but in addition, we identified the Kaena and Mammoth subchrons within the Gauss chron. Magnetic boundaries identification was made by assuming that the average magnetization on each side of a boundary has the same magnitude but an opposite sign (Figure 4) [Klitgord et al., 1975]. In this case, the magnetic boundaries are determined by relative zero levels. Owing to the sharpness of the transition (<0.5 km), defined as the area where 90% of the polarity change occurs [*Atwater and Mudie*, 1973], the errors associated with such determinations is likely to be negligible.

Identification of the main reversals was straightforward for all profiles. The resulting anomaly patterns (Figure 1) indicate that the spreading process has remained slightly asymmetric during the last 3 Myr, with 10% more new material being accreted on average to the Indian plate. Within each flank, no significant rate variation is observed between the profiles. The only difficulty occurs on the western side of profile B in the identification of the Kaena and mammoth subchrons within the Gauss chron (Figure 3), probably because of the presence of the Gasitao Ridge, a bathymetric feature which continues the Rodrigues Ridge eastward [*Dyment et al.*, 1999b] (Figure 1). A similar problem may affect profile s20 which crosses the Gasitao Ridge at its intersection with the CIR, resulting in unclear magnetic anomalies from the axis up to the Jaramillo subchron (Figure 1).

3.2. Spreading Axis Location

A precise location for the spreading axis (i.e., the zero-age crust) is required since we are looking for fine scale magnetic fluctuations and need a robust time calibration between profiles. On slow spreading ridges, active eruptive fissuring appears to be restricted to a narrow zone, ~2-km-wide, within the axial valley [*Ballard and van Andel*, 1977; *Macdonald*, 1982; *Brown and Karson*, 1988; *Gente et al.*, 1991; *Smith and Cann*, 1999]. The zone of active fissuring is even narrower (<1 km) on the fast East Pacific Ridge (EPR) [*Macdonald*, 1982; *Choukroune* et al., 1984; *Gente et al.*, 1986; *Fornari et al.*, 1998]. Previous studies have shown that a high magnetic anomaly generally occurs over the zone of most recent volcanism at fast or slow spreading rates (the so-called Central Anomaly Magnetic High (CAMH)) [e.g., *Klitgord*, 1976; *Macdonald*, 1977; *Hussenoeder et al.*, 1996; *Smith et al.*, 1999]. However, *Tivey and Johnson* [1987] noted that on the Juan de Fuca Ridge, newly erupted basalts locally coincide with a magnetic low as the result of extensive low-temperature alteration. Identification of the spreading axis based on the magnetic record must therefore be carefully checked against geological evidence (e.g., morphological

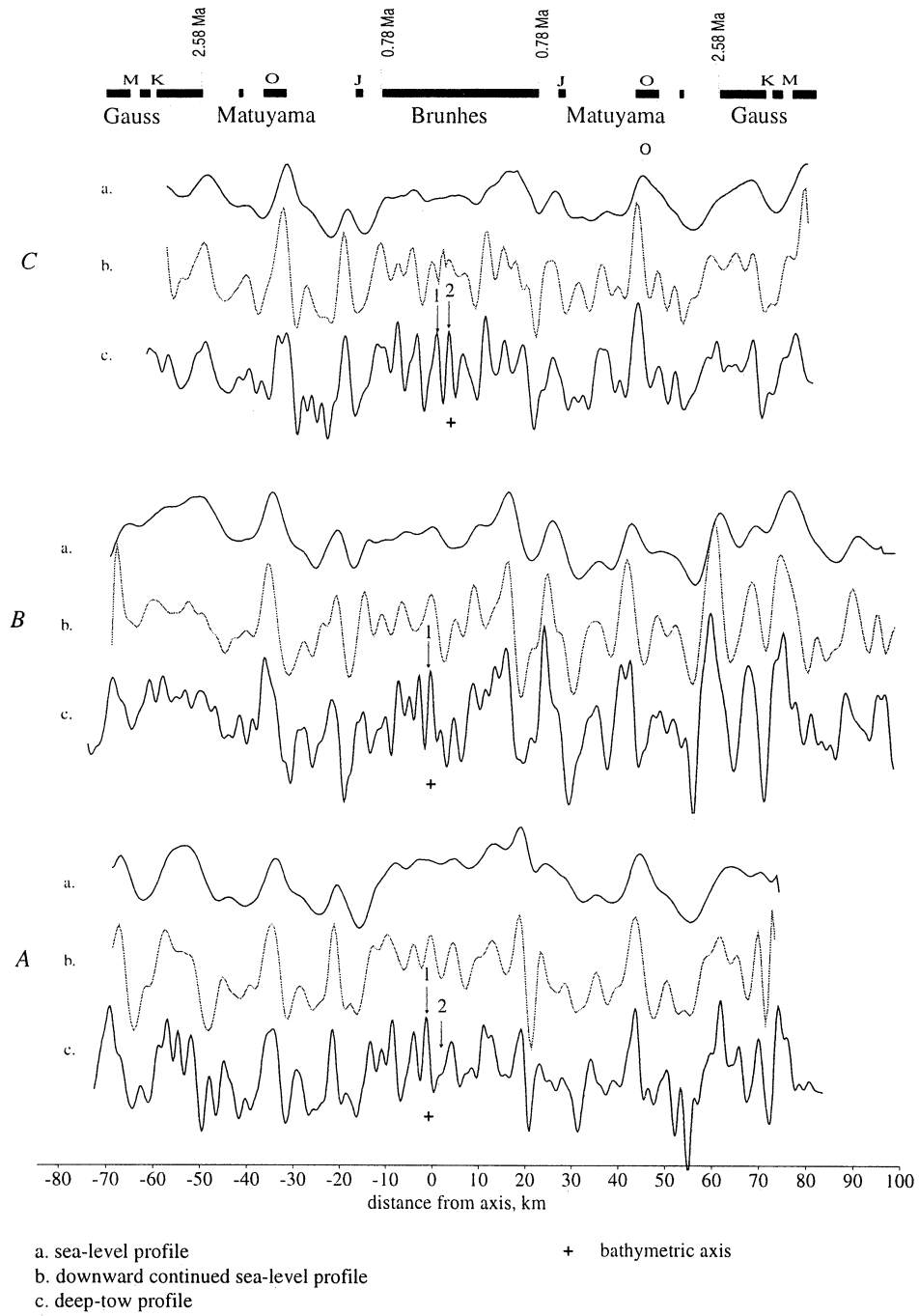

Figure 3. Comparison (a) for each deep-tow profile between the sea surface magnetic anomalies, (b) their downward continuation 2500 m below sea-level, and (c) the corresponding near-bottom profile. All magnetic profiles are reduced to the pole and corrected from topographic effects (profiles were calculated for a depth of 2000 m with a 2500-m-deep flat topography). Possible locations of the magnetic axis are numbered up to 2 and the cross indicates the bathymetric axis.

signature of an active volcanic ridge, axial zone of high seafloor reflectivity).

For the surveyed CIR area, most of the CAMH locations picked on downward continued sea surface profiles correspond to the bottom of the axial bathymetric valley and are therefore good approximations for the spreading axis location (indicated by crosses in Figure 4). However, the near-bottom magnetic profiles reveal a more complex situation sometimes with several highs with wavelengths <4 km in a narrow zone centered in the 5- to 10-km-wide median valley (Figure 3). There are, for instance, two magnetic highs in profile C (labeled 1 and 2 in Figure 3), which are both possible spreading axis locations whereas the corresponding sea surface profile of poorer resolution exhibits only one high with a 8- to 10-km wavelength. A blind identification of the axis, for which the profiles are expanded to a common spreading rate between the conjugate Brunhes and Matuyama boundaries (the axis is thus located at the middle of the

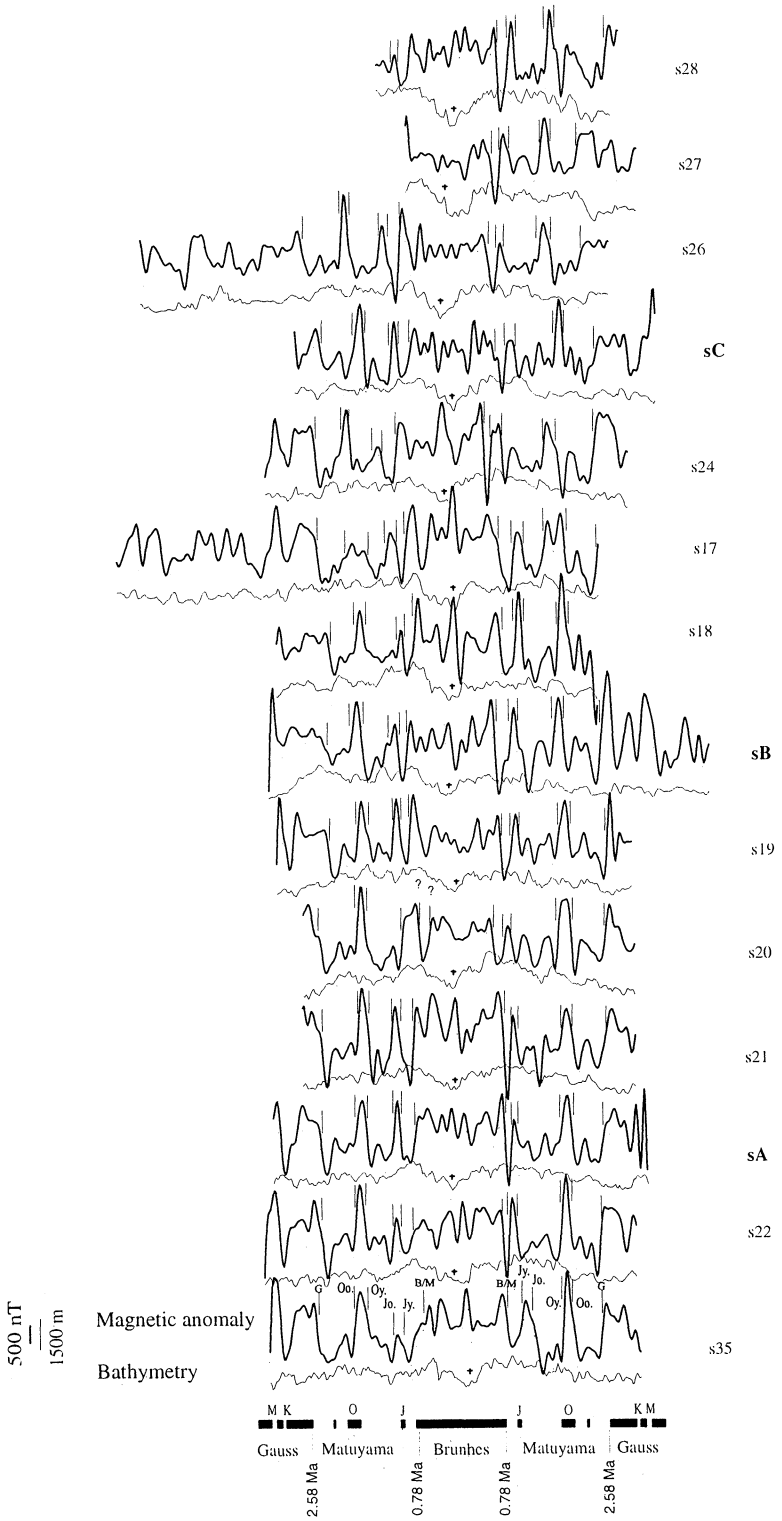

Figure 4. Downward continued sea-surface profiles and their corresponding bathymetry (thick lines). The cross shows the magnetic axis, determined as a magnetic high located within the axial valley (CAMH). The vertical lines indicate the polarity boundaries.

modified profiles), suggests that the central anomaly closely lies above the bathymetric valley (location 2 on Figure 3 and Figure 5a). This solution seems supported by analysis of the downward continued neighbouring sea surface profiles s24 and s26. However it is not confirmed by the reflectivity data available on the investigated area (D. Sauter and A. Briais, personal communication, 1999). These data show that the zone of maximal reflectivity is located 2.5 km away and corresponds to the magnetic high lying at location 1 (Figure 3 and Figure 5b). For profile C we therefore prefer to consider the axis location constrained by the reflectivity data.

The spreading axis is easily identified on profile B where there is only one magnetic high (3 km width, labeled 1 in Figure 3). This is also true for the downward continued

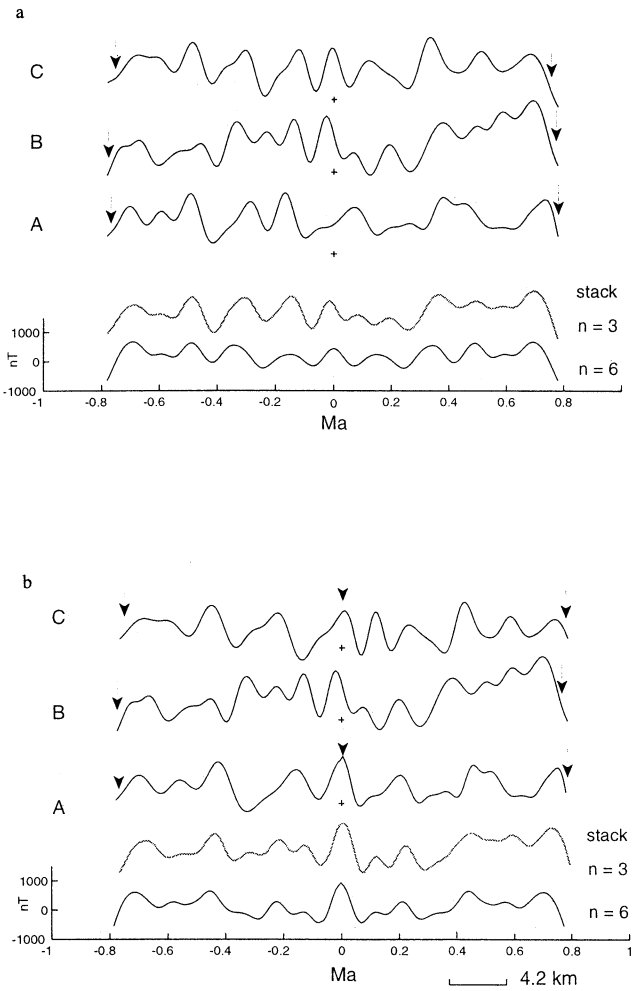

Figure 5. Possible locations of the spreading axis and stacks of the deep-tow magnetic anomaly profiles for the Brunhes chron. (a) Expanded profiles to a common rate between two tie points corresponding to the Brunhes-Matuyama boundaries (solid arrow). The cross indicates the spreading axis located at the middle of the profile (blind identification). (b) Locations of the chosen axes (see the text for discussion). In both cases, the curves at the bottom are the resulting stacked anomaly profiles for N=3 (the profiles from the eastern and western flanks are added separately) and N=6 (all profiles are added together).

neighboring profiles (sB, s18 and s19). For all these profiles the magnetic high clearly corresponds to the deepest part of the axial valley. Moreover, either the blind identification of the spreading axis (cross on profile B, Figure 5) and the reflectivity data, showing a strong reflective corridor within the median valley (D. Sauter and A. Briais, personal communication, 1999), support location 1 as being the true location of the spreading axis.

The situation is more ambiguous for the profile A. There are two possible axis locations over a distance of ~5 km (indicated by 1 and 2 on Figure 3). The first possibility (location 1) is a magnetic axis that corresponds to the deepest part of the axial valley. The blind identification locates the axis ~4 km away (location 2, Figures 3 and Figure 5a). If location 1 is chosen, the spreading rate would be strongly asymmetric during the Brunhes chron, with a faster expansion of the Indian plate; however, highly asymmetric spreading may be a common feature on slow spreading ridges [*Allerton et al.*, 2000]. This asymmetry is removed if location 2 is considered. The downward continued sea surface profiles s21 and s22, for which the axis is easily picked, argue in favor of locally asymmetric spreading within the Brunhes, thus supporting location 1. Moreover, the reflectivity data also strongly support location 1, with location 2 corresponding to a less reflective area at the foot of the eastern wall of the median valley.

Finally, in order to illustrate the uncertainties which may result from the different possible locations of the spreading axis, we have calculated stacked magnetic anomaly profiles for Brunhes considering in Figure 5a only the blind identification of the axis for each profile and in Figure 5b using our chosen locations. The comparison between the two stacks shows that differences exist only during the recent part of the Brunhes record (0.4 Ma to present), which must be thus considered with caution. Furthermore, the stack performed with the chosen axis locations yields a stronger CAMH (Figure 5b).

4. Identification of Short-Wavelength Anomalies

4.1. Stretching and Stacking the Near-Bottom Profiles

Once the principal magnetic polarity intervals have been clearly identified, it is possible to test whether short-wavelength anomalies observed on deep-tow magnetic profiles are consistent throughout the investigated area. This test was performed first by transforming the distances of magnetic profiles into time using the *Cande and Kent* [1995] geomagnetic polarity timescale and a linear interpolation between the identified reversals. In order to take into account effects of spreading asymmetry and possible ridge jumps, processing was made in three steps (referenced as steps 1, 2, 3), each step involving additional tie points. We have also considered separately the western and eastern portions of deep-tow profiles, and for each step of the processing we have calculated an average (stacked) magnetic anomaly profile (Figures 6a and 6b). In the first step (step 1), the stretching of the magnetic profiles was done using only three tie points: the axis (zero age), the Brunhes-Matuyama (0.78 Ma) and the Matuyama-Gauss (2.58 Ma) boundaries. Then we considered the following other tie points (step 2): the younger and older boundaries of the Jaramillo and Olduvai subchrons (0.99-1.07 Ma and 1.77-1.95 Ma), the mean age for the Kaena and the mammoth subchrons (3.07 and 3.27 Ma, respectively), and the Gauss-Gilbert boundary (3.58 Ma). Within the Brunhes chron, only step 1 is computed since the number of tie points was not changed. Finally (step 3), aware of the danger of circular reasoning, we tentatively considered as additional time markers a few evident small-scale anomalies between the Jaramillo and Olduvai subchrons, which are correlatable on both flanks (Figures 6a and 6b).

In sections 4.2-4.4 the consistent short-wavelength anomalies observed within the Brunhes, Matuyama, and Gauss chrons will be referenced with the label B, M, or G respectively. Negative microanomalies are mentioned when they occur within a normal polarity interval (Brunhes and C2An); in contrast, positive microanomalies are labeled when they are located within a reversed polarity interval (during the Matuyama chron).

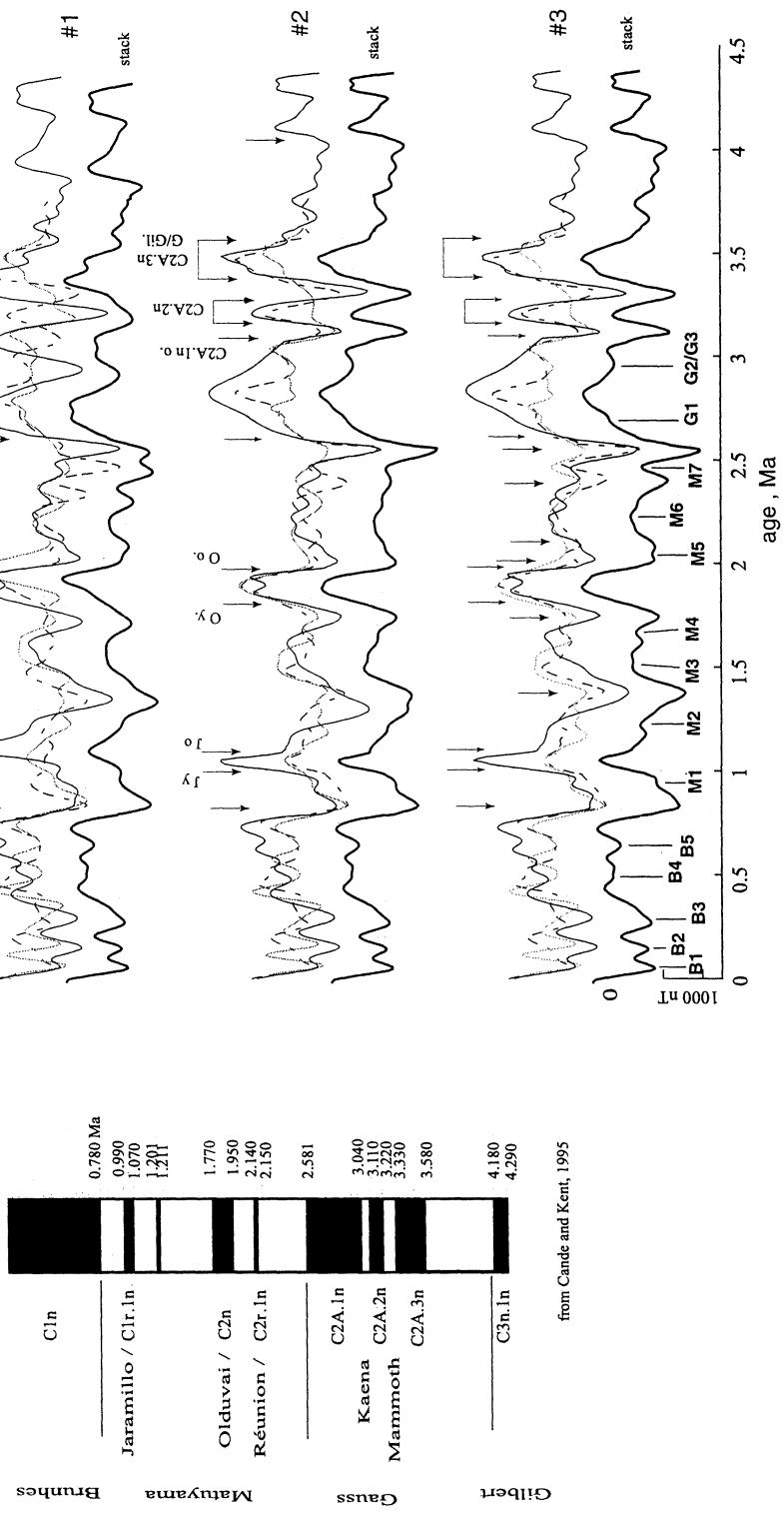

Figure 6a. Stacking of the eastern portion of the deep-tow magnetic anomaly profiles. The arrows indicate the tie points used to expand the profiles. (top) Stretch 1. We only consider the Brunhes-Matuyama and Gauss-Matuyama boundaries as tie points. (middle) Stretch 2. All well-known reversal boundaries are used as tie points. (bottom) Stretch 3. A few tiny wiggles between Jaramillo and Olduvai subchron and between Olduvai and Gauss are considered as additional time markers. For each stack order, the bottom curve (thick line) shows the averaged anomaly profile. Possible short-lived features are indicated on the stacked anomaly profiles (B1 to B5, within the Brunhes chron; M1 to M7, within matuyama; G1 to G3, within Gauss). Timescale is from Cande and Kent [1995].

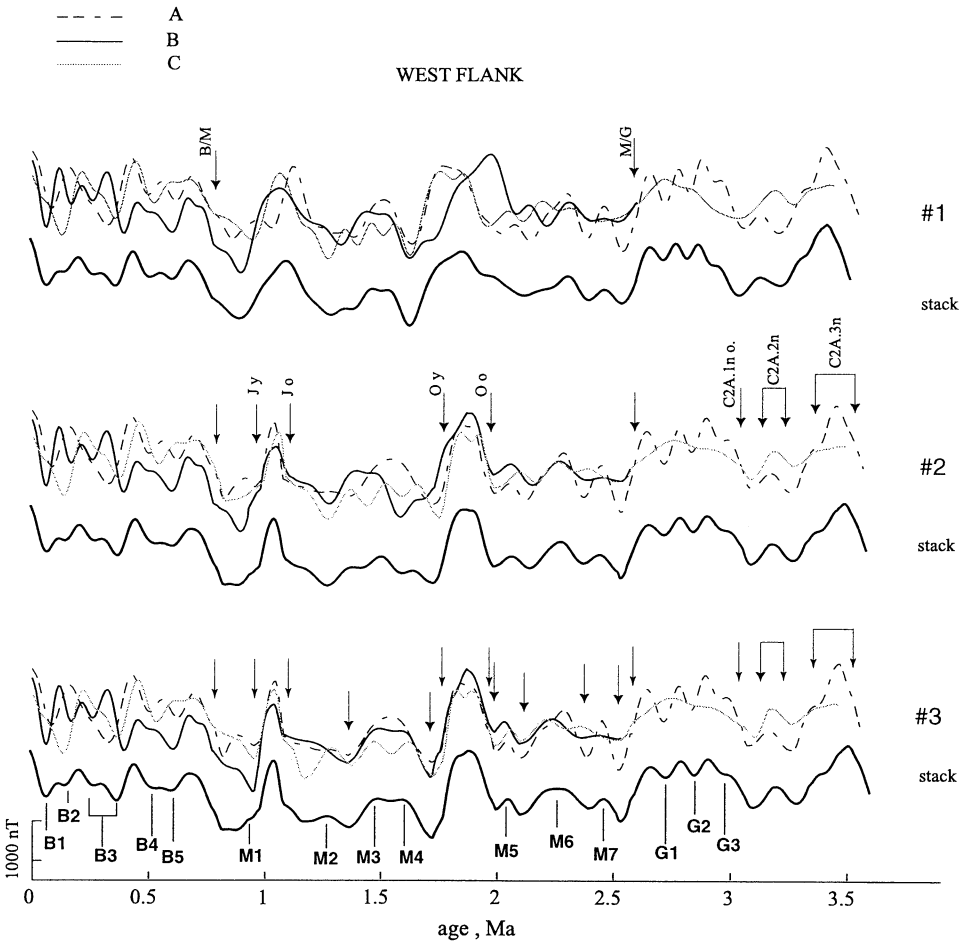

Figure 6b. Same as Figure 6a except for the western portions of the profiles.

4.2. Short-Wavelength Anomalies Within the Brunhes Chron

The two stacks obtained for the eastern and western sides of the CIR are very similar, with the same pattern of microanomalies (Figures 5b and Figures 6a and 6b). This similarity allows us to compute a general stack 1 for Brunhes combining the six available deep-tow profiles (Figure 7).

In addition to the CAMH, two well-developed magnetic highs, at ~0.45 Ma and 0.7 Ma, respectively, are observed, together with some features of smaller amplitude. Between the high at 0.45 Ma and the CAMH, at least three microanomalies are observed (labeled B1, B2, and B3 in Figures 6 and 7). The age of the end of the CAMH (B1) is roughly similar on both flanks (~60 ka on the east, and ~70 ka on the west) and is consistent between all the individual profiles. Within the older half of Brunhes, two additional anomalies (B4 and B5, Figures 6 and 7) are present.

4.3. Short-Wavelength Anomalies Within the Matuyama Chron

For the Matuyama chron the three deep-tow profiles along each flank of the CIR are rather consistent (Figures 6a and 6b). This is emphasized by the similarity in both cases between stacks 1, 2, and 3 for the two sides. Stack 3 naturally exhibits more pronounced features, but they are already apparent in stack 2.

Four individual or groups of short-wavelength anomalies are observed. The older group of microanomalies lies between the Matuyama-Gauss boundary and the Olduvai subchron. The western ridge flank yields a very regular record of these anomalies and stacks 2 and 3 on this flank are almost identical (Figure 6b). The situation is not as favorable on the eastern side, but the stack computed for this flank does not contradict the western one. We observe a dominant anomaly (M6) with two contiguous anomalies of smaller amplitude (M5 and M7). The older one (M7) is clearly present on both flanks (Figures 6a and 6b).

Between the Olduvai and the Jaramillo subchrons, two main features are found. The oldest appears as a relatively broad bump on both ridge flanks with an amplitude of ~1500 nT and a wavelength of ~8 km. The individual profiles from both flanks (Figure 6a and 6b) suggest that this anomaly is likely to result from several closely spaced events (at least two, M3 and M4) around 1.5 Ma instead of a single, longer-lasting event. Another anomaly is present just before the Jaramillo subchron at ~1.2 Ma (M2). This feature is particularly well developed on the eastern part of profile B (Figure 6a), in which the individual events are better resolved and the Jaramillo subchron has the highest amplitude.

The youngest anomaly (M1) recorded within the Matuyama lies at ~0.9 Ma, between the end of Jaramillo and the Matuyama-Brunhes boundary. The signal is of very short wavelength and low amplitude (~500 nT), and the anomaly is

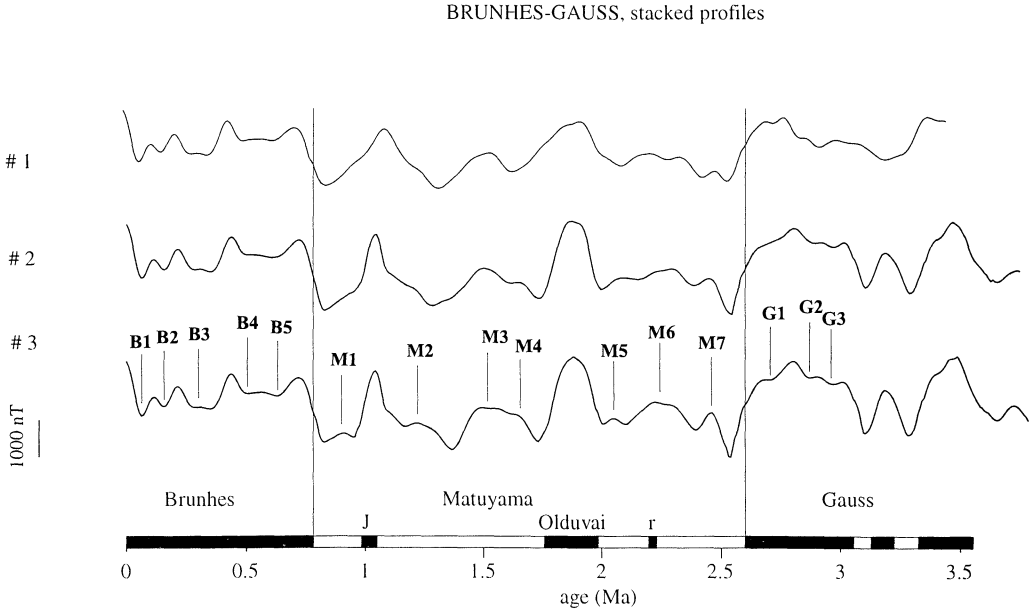

Figure 7. General stacked anomaly profiles from the six deep-tow records (three each side of ridge, except for step 3, where the western part of B has been omitted for the Gauss chron). Stretching orders (step 1 to step 3) are the same as in Figure 6. The identified short-lived events are indicated on the stacked profile 3.

obvious only on two profiles, in particular, the western and eastern parts of profiles A and B, respectively. On the stacks the resulting anomaly is characterized by a small bump in the youngest part of the Jaramillo anomaly, more pronounced on the eastern flank (Figure 6a) than on the western side (Figures 6b).

The similarity observed between the eastern and western stacks justifies the computation of a general stack from the 6 deep tow profiles across the Matuyama chron (Figure 7). This stack is very consistent whatever step is considered. Only the very tenuous anomaly M1 observed in stack 3 but not seen in stacks 1 and 2, seems questionable.

4.4. Short-Wavelength Anomalies Within the Gauss Chron

As previously pointed out, the Gauss chron part of the record is problematic for the western side of profile B, probably because of the presence of the Gasitao Ridge (Figure 1). We have thus eliminated this portion of profile B from stack computation (Figure 6b). For the other profiles the identification of the Kaena and mammoth subchrons is straightforward, although the anomaly amplitudes vary between the profiles (note the high amplitude of the signal for the eastern part of profile B, Figure 6a). The stacks obtained for the two flanks are similar, with three short-wavelength anomalies during the C2A.1n (labeled G1, G2, and G3 in Figures 6 and 7). On the eastern flank the presence of the event G1, closely preceding the Gauss-Matuyama transition, tends to give an apparently gradual (i.e., long-lasting) polarity change at the Gauss-Matuyama boundary. On both flanks, we also note the same asymmetric shape of the older normal polarity interval within the Gauss chron (the C2A.3n subchron, between 3.33 and 3.58 Ma), with a gradual decrease in amplitude after the Gilbert-Gauss boundary. The general stack computed from five profiles exhibits the same characteristics as above (Figure 7).

5. Testing the Regional Consistency of the Small-Scale Anomaly Sequence

We selected the sea surface magnetic profiles that yield a clear identification of the principal polarity intervals and/or that show no obvious bathymetric effect (Figure 8). Only the western parts of profiles s17 and s20 were excluded from the data set because of disturbed magnetic anomalies associated with rough bathymetry (Figure 8). The profiles were transformed into time using the Brunhes-Matuyama boundary, the younger and older boundaries of the Jaramillo and Olduvai subchrons and the Matuyama-Gauss boundary as tie points (equivalent to stretch 2 on the deep-tow data). Again, we first computed separately a stack for the western and the eastern flanks of the CIR (curve a in Figure 8), before adding the profiles together (curve b in Figure 8).

Within the Gauss chron the shape of the anomaly produced by the younger normal polarity interval (C2A.1n subchron) is similar after stacking of profiles from both ridge flanks, although those from the eastern side show more distinctively the occurrence of two short-wavelength anomalies (Figure 8). Between the Gauss chron and the Olduvai subchron, two events are observed from the western flank, but only one from the eastern flank is observed. Note that several profiles from this latter side clearly exhibit two distinct events (e.g., profile s18). The loss of one event may be due to small-scale spreading variations. Between the Olduvai and Jaramillo subchrons, two well-developed events are present on both flanks, the youngest one being more marked on the eastern side. Within the Brunhes chron, we observe that the anomaly amplitude decreases from the Brunhes-Matuyama boundary up to the end of the CAMH at ~0.11 Ma. Except for the CAMH, two magnetic highs are observed in all profiles on both flanks around 0.7 Ma and 0.4 Ma. The stack computed for the eastern ridge flank shows an additional small anomaly, slightly older than the CAMH.

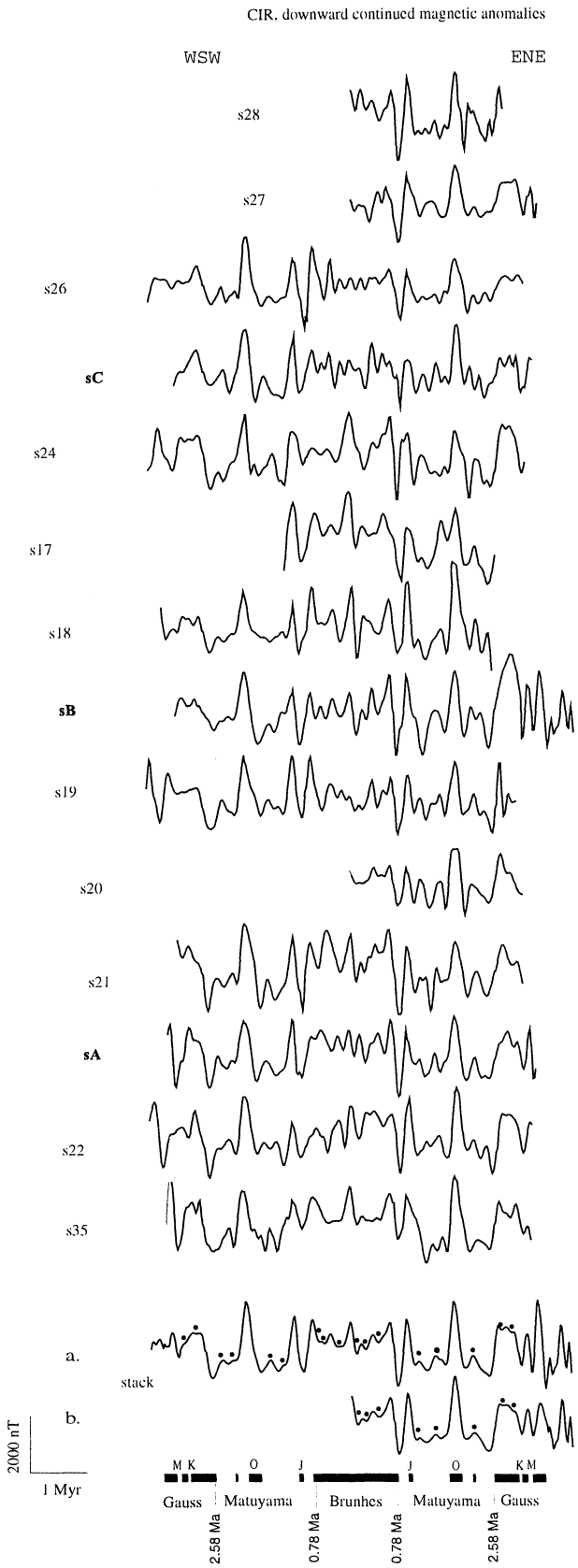

Figure 8. Downward continued sea surface magnetic profiles from the CIR with time as abscissa. Horizontal distance was converted to time by interpolating between fixed points at the Brunhes-Matuyama boundary, old and young boundaries of the Jaramillo and Olduvai events, and Matuyama-Gauss boundary. The two curves at the bottom are stacked profiles: curve a shows the west and east sections stacked independently, and curve b shows them stacked together. Solid dots indicate the possible short events (see text).

The small-scale anomaly pattern obtained from the downward continued profiles on the CIR is therefore similar to the one deduced from the three deep-tow profiles (compare Figure 8 curve b with stack 3 in Figure 7), although some parts of the signal may have been missed in the sea surface magnetic anomaly profiles. This indicates a regional consistency of the described short-wavelength anomalies and gives us confidence in interpreting them as real geomagnetic events.

6. Discussion

6.1. Worldwide Consistency of Short-Wavelength Anomalies From the Gauss to the Brunhes Chrons

In order to test the reliability of the short-wavelength magnetic anomalies found in the CIR area at even broader geographical scales, we considered two sets of sea surface profiles obtained from the EPR at 19°S [*Rea and Blakely*, 1975] and from the Pacific-Antarctic Ridge (PAR) between 53° and 66°S [*Géli et al.*, 1997].

The EPR and the PAR profiles were selected for the consistency of their magnetic patterns, low roughness bathymetry, and their different spreading rates (~75 km/Myr average half rate for the EPR and ~35 km/Myr for the PAR). The PAR magnetic anomalies have a low theoretical and observed degree of skewness (~2°) because of their high latitude and the near north-south strike of the ridge. Each profile was deskewed with the phase-shifting method of *Schouten and McCamy* [1972]. In contrast, the EPR magnetic anomalies profiles have a significant skewness despite the low theoretical value (~8°). This skewness was removed from each individual profile using a large range of angles (from +5° to –50°, with lower values in the northern and southern parts of the surveyed area) and the associated amplitude factors for taking into account local variations of the lineation strike. In order to compare the profiles from the PAR, the EPR, and the CIR, we applied the same processing as before: each profile was topography-corrected using the *Parker and Huestis* [1974] method (the inversion was performed with a 500-m source thickness and a 3-km short-cut wavelength) and recomputed 2000 m below sea level with a flat topography at 2500 m. The spreading rate in the PAR investigated area increases from south to north, the full spreading rate changing from 54 km/Myr at 65°S to 74 km/Myr at 55°S [*Géli et al.*, 1997]. Spreading on the EPR shows an asymmetry of ~10 %, with a higher rate on the eastern flank. Eleven and 12 profiles were processed on the eastern and western flanks of the EPR, respectively, whereas 19 and 11 profiles were considered for the two flanks of the PAR (Figure 9). All profiles were transformed into time using the same tie points as for stack 2 computed for the CIR profiles. For both regions we first computed an average profile for each ridge flank before stacking all the profiles (Figure 9). For comparison, we have computed stacked anomalies of the sea surface profiles and of the downward continued profiles, i.e., anomalies computed at 2000 m depth.

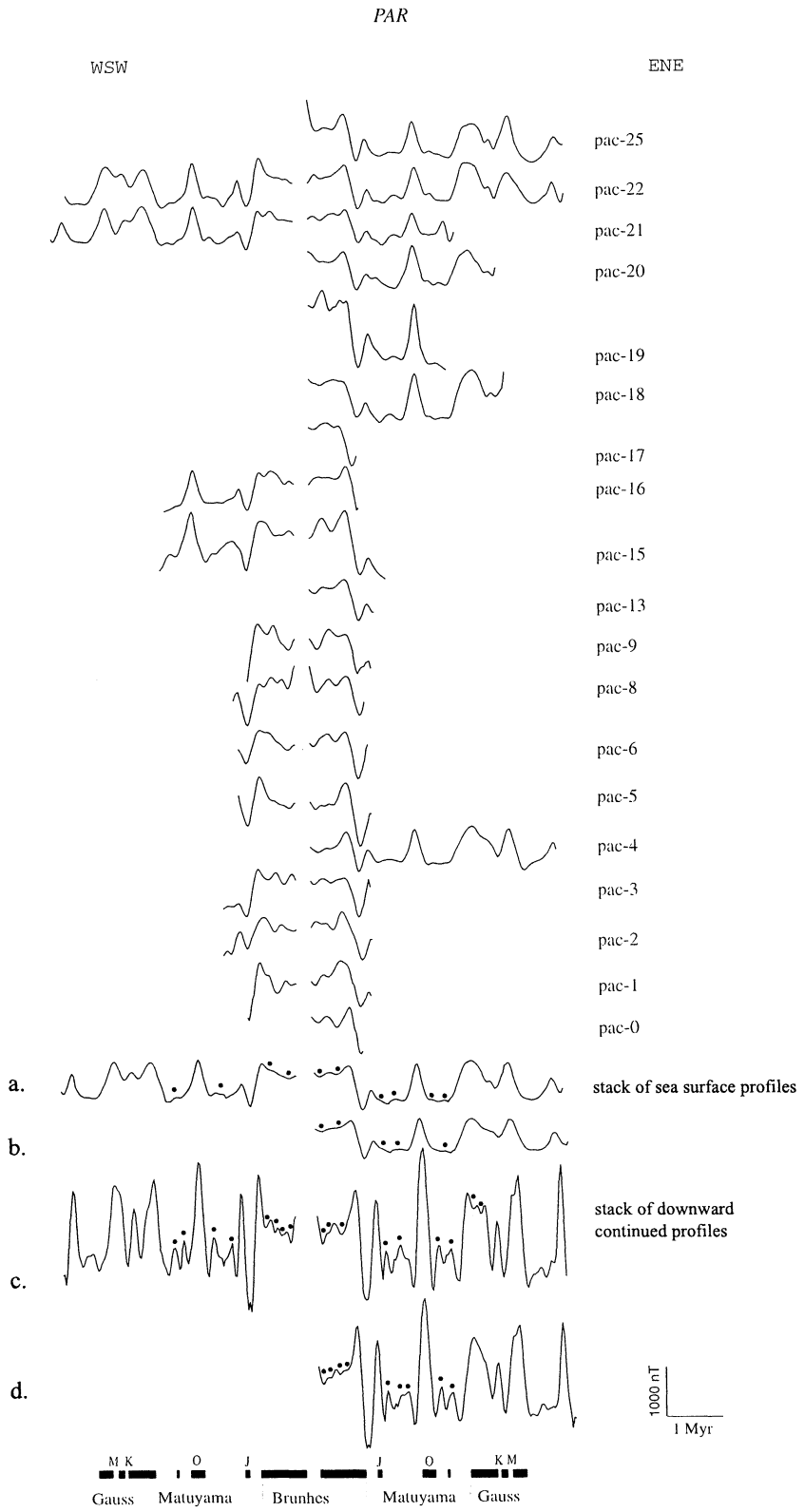

Figure 9. Sea surface magnetic profiles on the EPR at 19.5°S and on the PAR (centered at 60°S), plotted from south to north. We use the NOAA pol7302 and pol7303 surveys (NGDC 03040059 and 60) data for the EPR and the PARANTARCTIC survey (1996, 96010020) on R/V *l'Atalante*. All the profiles are adjusted to a common spreading rate (80 km/Myr for the EPR and 35 km/Myr for the PAR) and axis centered. Curves at the bottom are the stacked magnetic anomaly of sea surface profiles (curve a, independent stacked; curve b, east and west sections together) and downward continued profiles (curve c independent stacked; curve d, east and west sections together). Solid dots indicate possible short events (see text).

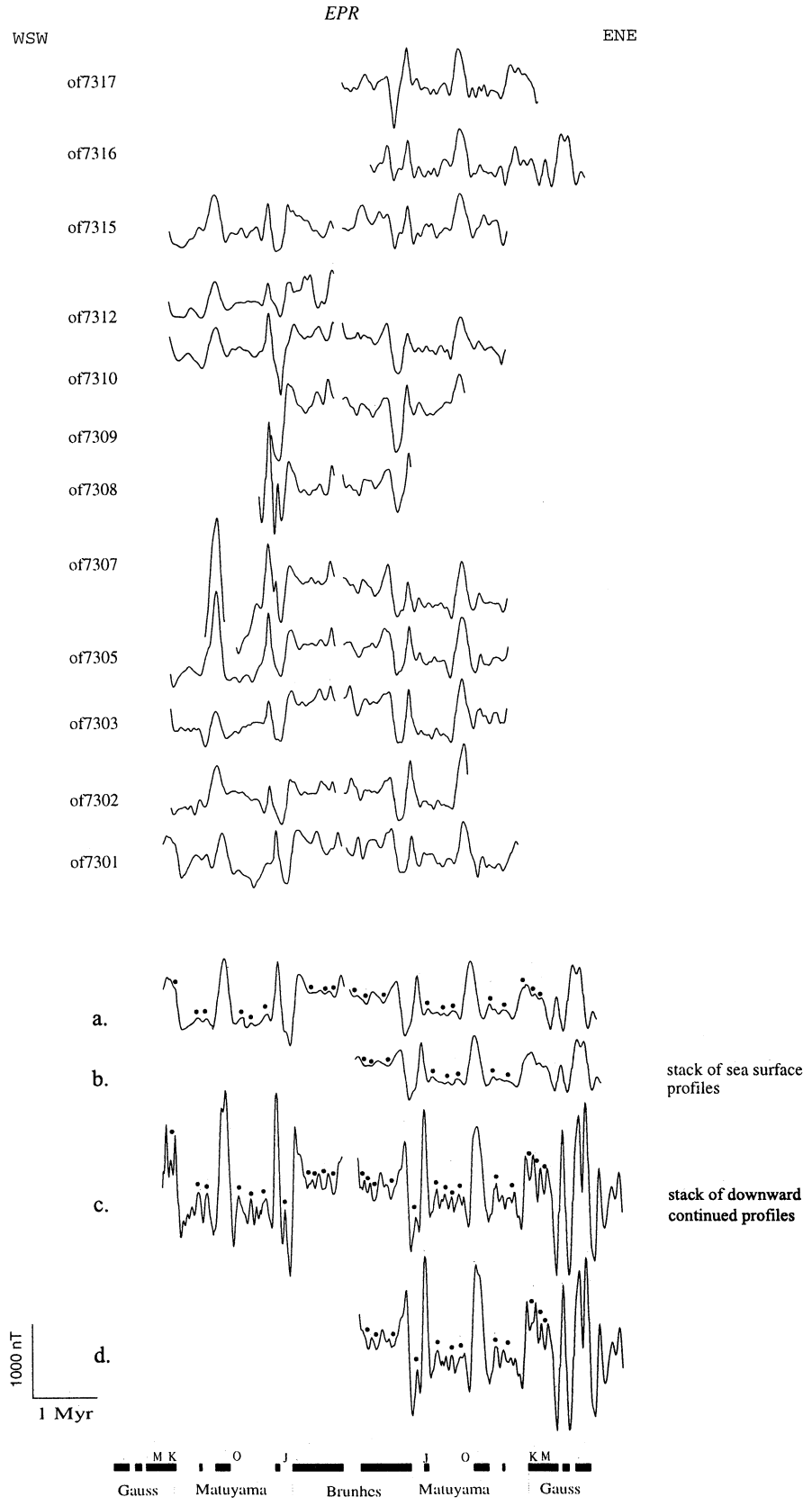

Figure 9. (continued)

Similarities clearly exist between the EPR, the PAR, and the CIR stacked profiles (Figures 8, 9, and 10). The downward continued profile from the EPR yields the record with the highest time resolution, whereas the EPR sea surface stacked profile fits very well with the downward continued profile from the CIR. Compared to the EPR and to the CIR deep tow profiles, the small-scale magnetic anomalies from the PAR have smaller amplitudes, but they show a similar anomaly pattern (Figure 10).

For the three ridge systems the sea surface profiles and their downward continuation show a gradual decrease in amplitude from the Brunhes-Matuyama boundary up to the beginning of the CAMH, with the occurrence of several short-wavelength anomalies. Note that the downward continued profile obtained from the eastern part of the EPR provides a microanomaly pattern (anomalies B1, B2, B3 and gathered B4-B5) comparable to the one found from the CIR deep tow record (B1-B5). In all cases, the number of microanomalies occurring within Brunhes is similar and, depending on the degree of resolution, is between 3 and 5. For the Matuyama chron the profiles from the EPR and the PAR confirm the occurrence of several anomalies between the Gauss-Matuyama boundary and the Olduvai subchron and between Olduvai and Jaramillo. The downward continued PAR profile yields a very distinct sequence of small-scale anomalies, which clearly confirms the existence of one well-defined anomaly just after the Olduvai subchron as found from the CIR deep-tow data (M3 plus M4). The downward continued EPR profile further supports the reliability of the microanomaly (M1) previously suggested between Jaramillo and the Brunhes-Matuyama boundary. Finally, the anomaly corresponding to the C2An.1n subchron within Gauss shows exactly the same shape in all cases, marked by a high amplitude during its youngest half. There are likely to be three microanomalies within the C2An.1n subchron (EPR and CIR deep-tow profiles).

One important observation from this study is therefore the good correspondence of the near-bottom and downward continued stacked profiles from the CIR on one hand and between the stacked profiles from the EPR and PAR on the other. Together they indicate that at least most of the short-wavelength anomalies identified from our CIR deep-tow profiles within the Brunhes, Matuyama, and Gauss chrons are global phenomena and thus have a geomagnetic origin.

Before the discussion in section 6.2, one important remark must be made regarding the fact that if deep-tow results are helpful for detecting short-lived geomagnetic features, the clear distinction between subchrons and geomagnetic excursions from such data appears to be extremely difficult. Assuming that the intensity of the geomagnetic field is fully recovered during short magnetic polarity intervals, this would require the acquisition of very high resolution magnetic anomaly profiles from widely distributed spreading ridge systems. At present, we cannot discrimate between these two types of geomagnetic events.

6.2. Comparison Between Deep-Tow and Paleointensity Data

Paleointensity results are now relatively numerous for the Brunhes chron. They have been recently reviewed by *Guyodo and Valet* [1999], who performed a stacked composite record from a set of 32 widely distributed marine sediment sequences. In their report, they combined a previous stacked record over the last 200 kyr [*Guyodo and Valet*, 1996] with a new one spanning the older 600 kyr of the Brunhes chron. Magnetization was normalized between all the sequences in order to provide a continuous and homogeneous relative paleointensity curve, partly calibrated with a reference curve of $\delta^{18}O$. Paleointensity data are more scarce for the matuyama chron. Two data sets are presently available: one by *Valet and Meynadier* [1993] for the equatorial Pacific (Ocean Drilling Program (ODP) Leg 148), which extends up to the middle of the Gilbert chron (4 Ma), and another by *Kok and Tauxe* [1999] from the Ontong Java Plateau (ODP leg 130). In both cases, the sedimentation rates (~2-3 cm/kyr) were assumed to be low enough to average out nondipole field components, and therefore they are thought to reflect dipolar field intensity fluctuations.

The comparison between the CIR deep-tow magnetic results and paleointensity data is made here by forward modeling of the anomalies with the CIR spreading rate using the paleointensity variations as a modulation of the seafloor magnetization. The models are constructed from a sequence of magnetization blocks of 2000 years duration, the sign of these magnetization blocks being changed only for the well-known reversed polarity intervals. Two models are considered: one is constructed from the Brunhes to Gauss sequence obtained by *Valet and Meynadier* [1993] and the second by combining the stacked Brunhes record proposed by *Guyodo and Valet* [1999] with the Matuyama record obtained by *Kok and Tauxe* [1999]. In both cases, the variable magnetization is convolved with a 1.6-km gaussian filter (σ=1.6 km, R=0.7 [*Tisseau and Patriat*, 1981]) in order to simulate crustal emplacement (Figure 11). Synthetic profiles are computed with the same parameters as those used to correct the deep-tow magnetic profiles for topographic effect and phaseshift (flat bathymetry, survey at 2000 m below sea level, and a 500-m-thick magnetic layer). It is emphasized that this is an end-member modeling, for which all the details of the magnetic anomaly profiles are caused by geomagnetic field variations (i.e., changes in magnetization depend only on fluctuations of the geomagnetic field intensity).

Comparison in Figure 11 between the raw paleointensity data obtained by *Valet and Meynadier* [1993] and the corresponding synthetic magnetic anomaly profile shows that only the detection of major geomagnetic fluctuations, chrons, subchrons, and excursions can be expected from our near-bottom marine magnetic profiles due to their time resolution. Moreover, the saw-tooth pattern in paleointensity variations proposed by *Valet and Meynadier* [1993], in particular during the C2An.1n subchron (within Gauss) and between the Gauss-Matuyama boundary and the Olduvai subchron, cannot be clearly resolved in the CIR synthetic profiles, again because of the limited time resolution.

6.2.1. Brunhes chron. The near-bottom stack from the CIR shows three magnetic highs during the older (~0.70 Ma), middle (~0.45 Ma), and recent (CAMH) parts of the Brunhes chron which may correspond to periods of high geomagnetic field intensity (Figures 6, 7, and 11). Between the two older highs, there is a relatively long-standing low including the two microanomalies B4 and B5, between ~0.50 Ma and ~0.65 Ma. A similar low is observed between ~0.27 Ma and 0.37 Ma (microanomaly B3). The recent (~0.25 Ma to the present) part of Brunhes is marked by several highs and lows, which may

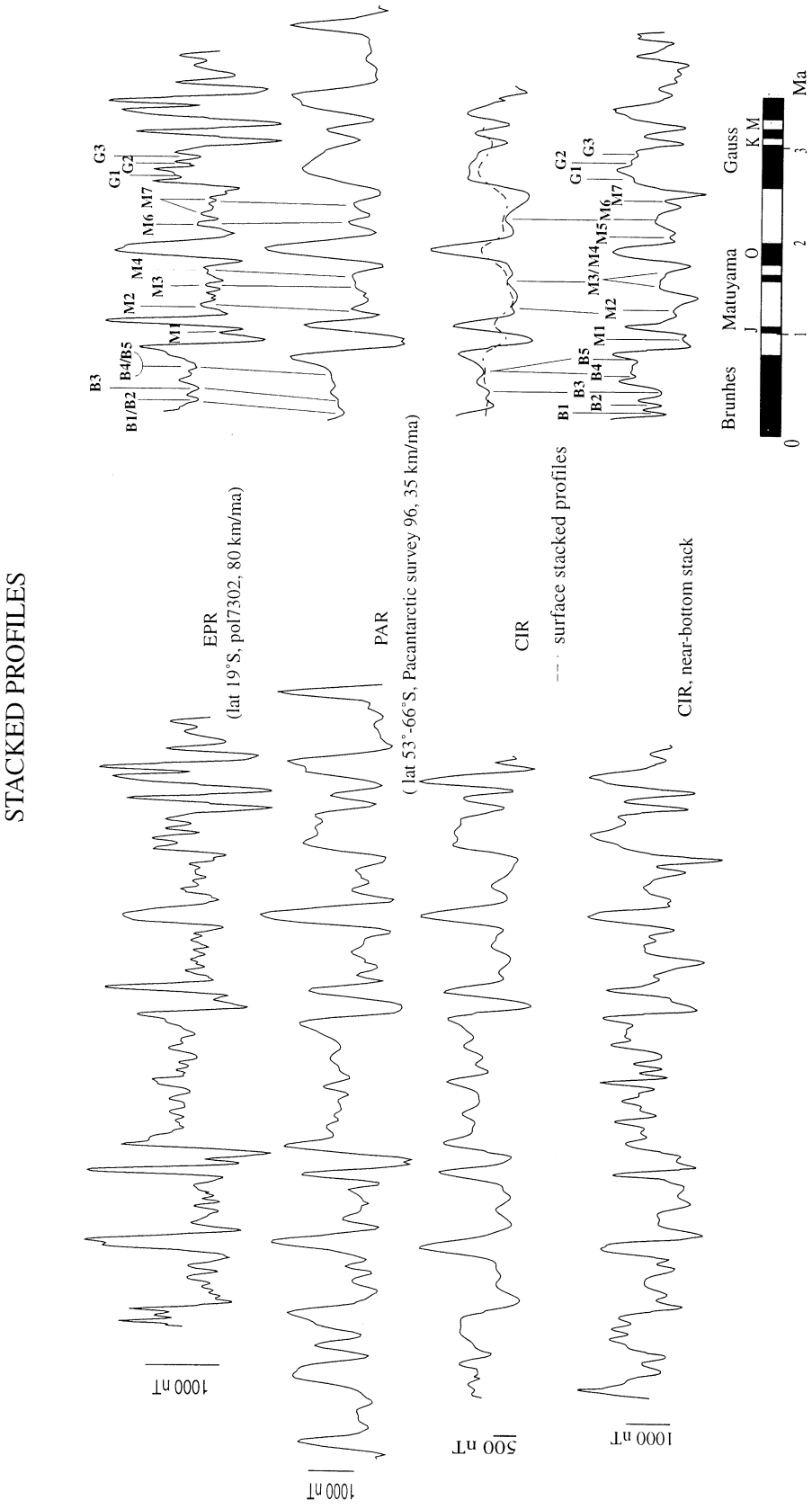

Figure 10. Comparison of the small-scale anomaly pattern from different ocean basins. (left) Stacked profiles from the EPR, the PAR, and the CIR separating in each case the profiles from the two ridge flanks. (right) Profiles from both added together. For the CIR the sea surface stacked profile (dashed lines) and its downward continuation (solid line) are represented on the same plot. Anomalies referenced B1 to G3 are discussed in the text.

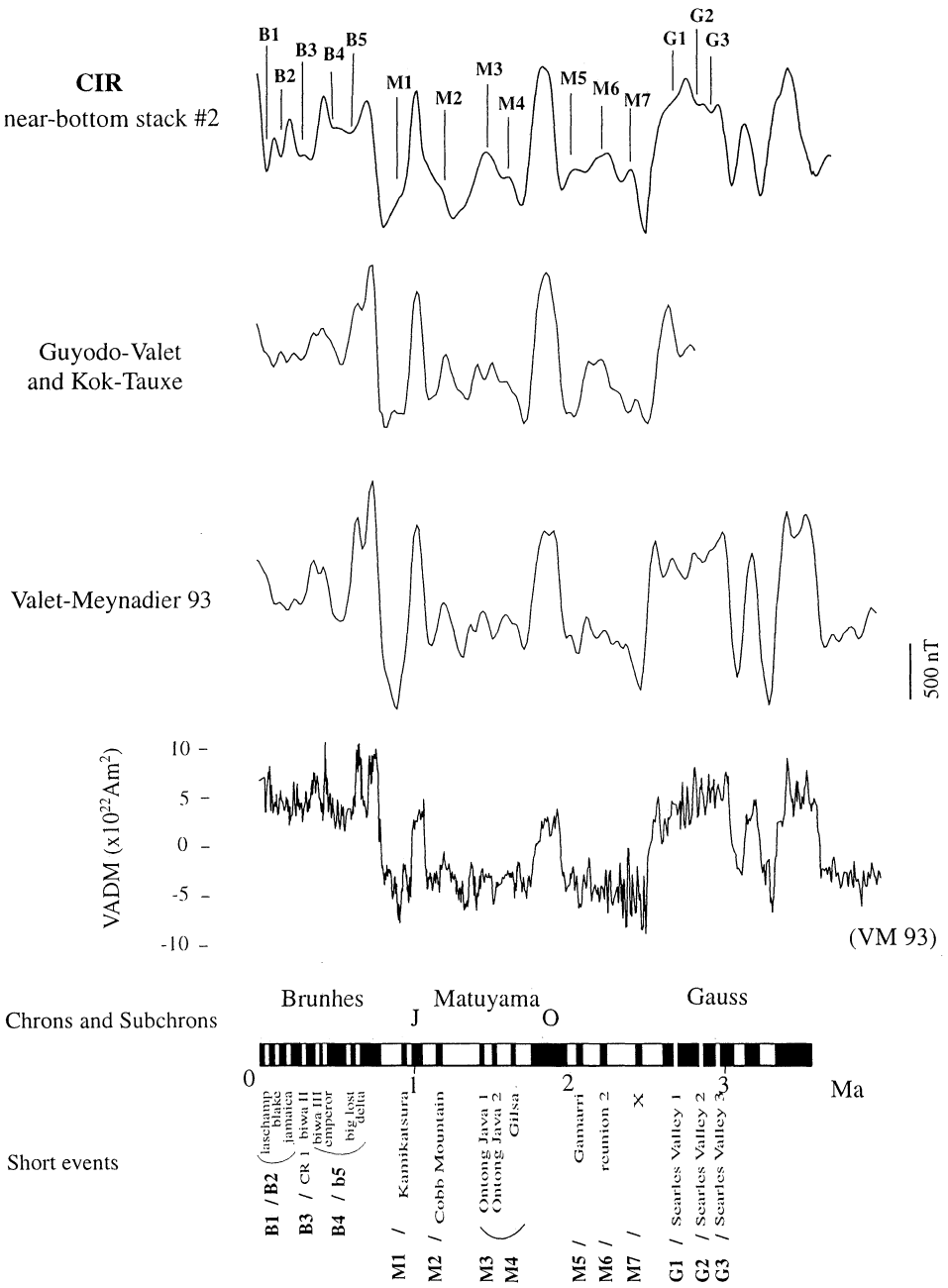

Figure 11. Comparison between the CIR near-bottom stacked profile and two paleointensity-based models constructed from data obtained by *Valet and Meynadier* [1993], *Guyodo and Valet* [1999], and *Kok and Tauxe* [1999]. The synthetic profiles are calculated with a flat bathymetry 2000 m below the sea surface and with a polarity transition width of 1.6 km. The raw paleointensity data obtained by *Valet and Meynadier* [1993] are also shown (VM 93; VADM is virtual axial dipole moment). Labels B1 to G3 indicate short-wavelength anomalies identified on the CIR deep-tow profile. For comparison, short events previously observed from magnetostratigraphic studies are marked on the geomagnetic polarity timescale.

indicate the occurrence of large and rapid paleointensity fluctuations (anomalies B1 and B2).

Direct comparison between the near-bottom profile and the paleointensity-derived models shows some differences either in terms of relative amplitude or precise location of the microanomalies. In the CIR near-bottom results, there is an unusual high-amplitude event during the middle part of Brunhes (between B3 and B4), which appears as an exception compared to the regional stacked profiles (CIR, PAR, and EPR) and to the synthetic profiles. Several factors may help to explain these discrepancies such as the sign (i.e., the polarity) of the geomagnetic field during excursions, which may drastically change the amplitude of the corresponding short-wavelength anomalies (in our modeling, the polarity of the geomagnetic field was not changed for any excursion) and/or problem in data reduction due to drastic changes of topography. Nevertheless, we observe in the synthetic profiles, as for the CIR deep tow profile, the occurrence of

several closely spaced small-scale anomalies during the more recent part of Brunhes. These microanomalies, which are slightly better developed in the Guyodo-Valet model than in the Valet-Meynadier model, are possibly related to the Laschamp (~0.04 Ma), the Blake (~0.12 Ma) and the Jamaica-Springle Falls (~0.19 Ma) excursions. The microanomaly associated with Laschamp is rather tenuous in the model, being partially masked by the CAMH, and may be missing in the deep-tow record where the CAMH is strongly marked. In this case, the two anomalies B1 and B2 in the CIR record, centered at ~0.06 Ma and ~0.15 Ma respectively, may correspond to the Blake and the Jamaica-Pringle Falls events. In this context, we note that *Emilia and Heinrichs* [1972] have already suggested that the Blake event is recorded in sea surface marine magnetic anomalies. The two models do not properly reproduce the high amplitude of the CAMH of the near-bottom profile (Figure 10). This may be consistent with the possibility that geomagnetic intensity variations are not the only contributor to the CAMH and that some differential alteration effects and/or magnetic properties variations are also involved [e.g., *Gee and Kent*, 1994; *Schouten et al.*, 1999; *Lee et al.*, 1996]. Alternatively, the amplitude of the CAMH could be considerably modified in the models by changing the sign of the field during the Laschamp and the Blake excursions.

The microanomalies observed before (B4 and B5) and just after (B3) the mid-Brunhes magnetic high can also be linked with the paleointensity data. Paleointensity records obtained by *Schneider and Mello* [1999] and *Guyodo et al.* [1999] suggest the occurrence of a period of low field intensity around 0.3 Ma, and *Langereis et al.* [1997] also found evidence for a geomagnetic excursion in Mediterranean sediments at the same age (Calabrian Ridge 1 event). This magnetic feature, which is, however, less obvious in the composite sequence proposed by *Guyodo and Valet* [1999], may be responsible for our microanomaly B3. Finally, the two anomalies B4 and B5 are likely to be related to the occurrence of several excursions between ~0.5 Ma and ~0.7 Ma (Calabrian Ridge 2-West Eifel, Big Lost-Emperor, La Palma, and Delta excursions [e.g., *Champion et al.*, 1988; *Langereis et al.*, 1997; *Guyodo and Valet*, 1999]).

6.2.2. Matuyama chron. In the deep-tow stacked profile the Matuyama chron exhibits a dense succession of short-wavelength magnetic anomalies between each subchron: M1 (~0.9 Ma), M2 (~1.2 Ma), M3-M4 (~1.3-1.6 Ma), M5 (~2 Ma), M6 (~2.2 Ma), and M7 (~2.4 Ma). The geomagnetic origin of the tenuous microanomaly M1 between the Brunhes-Matuyama boundary and the Jaramillo subchron (Figures 6, 7, and 11) is suggested by the synthetic profile computed with the *Kok and Tauxe* [1999] data, which show a similar anomaly. In contrast, the profile computed with the *Valet and Meynadier* [1993] results does not show any particular feature, although there is a low intensity around 0.93 Ma. This low, which is followed by a period of relatively high intensity, is well-marked in paleointensity data, but it is masked in the anomaly profile. Recent magnetostratigraphic studies have reported the occurrence of two successive very short geomagnetic events between the Brunhes-Matuyama boundary and Jaramillo, namely, the Kamikatsura and the Santa Rosa events, dated at ~0.88 Ma and ~0.92 Ma, respectively [*Singer et al.*, 1998; *Guyodo et al.*, 1999]. In this case, microanomaly M1 observed on the CIR could correlate with these two features.

All the stacked profiles show a consistent small-scale anomaly slightly older than the Jaramillo subchron (M2, Figures 6-11). The age interpolated for this anomaly, ~1.2 Ma in each case, suggests that it corresponds with the Cobb Mountain event. This magnetic polarity interval was first observed from marine magnetic anomalies [e.g., *Rea and Blakely*, 1975] and was later found in magnetostratigraphic studies of sediments and basalts [e.g., *Mankinen et al.*, 1978; *Clement and Kent*, 1987]. The CIR deep-tow data match reasonably well with a simple block model incorporating a 10,000-year-long normal polarity interval with a constant magnetization at 1.2 Ma. However, magnetostratigraphic results obtained from deep-sea sediments indicate that the duration of the Cobb Mountain event is likely longer, perhaps ~25,000 years [*Clement and Kent*, 1987; *Gallet et al.*, 1993]. The paleointensity data obtained by several authors [e.g., *Valet and Meynadier*, 1993; *Guyodo et al.*, 1999; *Kok and Tauxe*, 1999] all show a period of low field intensity around 1.2 Ma, with some evidence for a field recovery during the middle of this interval [*Gallet et al.*, 1993]. The two synthetic profiles exhibit a pronounced anomaly associated with the Cobb Mountain event. Although the polarity of the geomagnetic field was not changed during this interval, this anomaly is strongly more developed in the models than in the CIR near-bottom profile. This could be due to the occurrence of two closely spaced low field intensity intervals associated with the Punaruu event at ~1.1 Ma and the Cobb Mountain subchron itself [*Singer et al.*, 1998; *Guyodo et al.*, 1999], not recorded by either *Valet and Meynadier* [1993] or *Kok and Tauxe* [1999]. Another point here concerns the difficulty of distinguishing between subchrons and excursions. Among all the detected tiny wiggles, the Cobb Mountain event, which is observed worldwide in sedimentary and volcanic sections, probably corresponds to a true short magnetic polarity reversal interval rather than to an excursion. However, on the CIR deep-tow profile (and on the sea surface stacked profiles from the CIR, the EPR, and the PAR, Figure 10) the corresponding small-scale anomaly does not present a particularly high amplitude compared with other microanomalies which are related to excursional events.

An interesting and new feature is the occurrence of a consistent magnetic anomaly M3-M4 between Cobb Mountain (M2) and Olduvai both on the near-bottom profile and on the sea surface stacked profiles from the CIR and the EPR (Figures 6-11, M3-M4). This anomaly has a larger amplitude than the anomaly associated with the Cobb Mountain subchron. This is the first time that such a clear marine microanomaly is documented between 1.4 and 1.6 Ma. The comparison between the near-bottom results and the paleointensity-derived models is particularly good in terms of both wavelength and amplitude. Note that the fit is almost perfect with the *Kok and Tauxe* [1999] results. As mentioned earlier, the character of the CIR and EPR near-bottom signals suggests that this anomaly is, in fact, generated by a succession of at least two geomagnetic events (M3 and M4). This is supported by the available paleointensity data, which show three periods of low field intensity associated with the Ontong Java 1 and 2 and the Gilsa events [*Gallet et al.*, 1993; *Valet and Meynadier*, 1993] (see also *Guyodo et al.* [1999] for the youngest Ontong Java event). To date, large changes in geomagnetic direction have only been found for the event slightly younger than the Olduvai subchron, identified as

Gilsa by *Liddicoat et al.* [1980] and *Clement and Kent* [1987]; however, the excursional nature of the geomagnetic field also seems very probable for the two other events.

The CIR deep-tow profile shows three short-wavelength anomalies between the Oduvai and the Gauss-Matuyama boundary (M5, M6, and M7, Figures 6, 7, and 11), the youngest one (M5) having a very small amplitude (Figures 10 and 11). In the CIR, EPR, and PAR sea surface stacked profiles, there are two distinct microanomalies, which likely correspond to the "X" and "W" anomalies recognized earlier by *Heirtzler et al.* [1968], *Emilia and Heinrichs* [1969, 1972], and *Rea and Blakely* [1975]. These features are better known as the Réunion geomagnetic events, where at least one occurs in a volcanic section [*McDougall and Watkins*, 1973]. The comparison between the deep-tow and the synthetic profiles is again satisfactory, especially with the *Kok and Tauxe* [1999] derived model. For this data set, one prominent anomaly fits very well with the intermediate anomaly M6 ("W") observed in the near-bottom results. Another anomaly of smaller amplitude M7 ("X") occurring just after the Gauss-Matuyama can also easily be correlated between the deep-tow and the synthetic profiles (Figure 11).

The number and the ages of the Réunion events have long been debated (e.g., see *Emilia and Heinrichs* [1972] and *Kidane et al.* [1999] for a brief review). *Kidane et al.* [1999] dated by K/Ar method a geomagnetic event at 2.07±0.05 Ma in the Gamarri volcanic section in Ethiopia. A K/Ar date of 2.07±0.02 Ma was also obtained for a normal polarity interval from Réunion Island [*McDougall and Watkins*, 1973] but was later re-dated at 2.14±0.03 Ma by the Ar/Ar technique [*Baksi et al.*, 1993]. In the Gamarri section a period of low field intensity with transitional directions is observed before the interval of normal polarity, which might correspond with the ~2.14 Ma event [*Carlut et al.*, 1999]. This is further supported by the occurrence of two low paleointensity intervals at roughly 2.04 Ma and 2.14 Ma in the sequence obtained by *Valet and Meynadier* [1993]. This also suggests a geomagnetic origin for the youngest magnetic anomaly M5 observed in the CIR near-bottom profile (with an interpolated age of ~2.04 Ma). In any case, the prominent micro-anomaly M6 corresponds to the classic Réunion event between 2.1 and 2.2 Ma (C2r.1n [*Cande and Kent*, 1995]), which is probably a subchron, and the microanomaly M7 to another geomagnetic event between ~2.3 and 2.4 Myr. These considerations indicate that there are probably three geomagnetic events between the Gauss-Matuyama boundary and the Olduvai subchron. It is also of interest to point out that the general trend of the CIR deep-tow profile between the Gauss-Matuyama boundary and the Olduvai subchron is to the first order in good agreement with the synthetic profile constructed from paleointensity data showing a clear saw-tooth pattern.

6.2.3. Gauss chron. In contrast with the previous time interval, the synthetic profile constructed from the only sequence covering the Gauss chron cannot be satisfactorily correlated with the CIR deep-tow profile, in particular for the C2An.1n subchron (nor with the EPR or the PAR stacked sea surface and downward continued profiles). In the near-bottom profile its shape is almost opposite to that of the synthetic profile and thus does not support the gradual paleointensity decrease observed by *Valet and Meynadier* [1993]. There may be two explanations for this apparent disagreement. One is that the paleointensity data determined for this period, which have not been confirmed by independent data from another location, do not truly reflect the fluctuations of the geomagnetic field. The other is that the deep-tow magnetic profile is affected by unrecognized, tectonic or other processes, aside from those evident on the western side of the deep-tow profile B which crosses the Gasitao Ridge and was not used for the stack. The very good agreement obtained for this time interval between the profiles from the three ridge systems, including the stack computed by *Westphal and Munschy* [1999], from sea surface profiles from the EPR, argues in favor of the first alternative. If this explanation is correct, it would suggest that there are three short-wavelength anomalies during the C2An.1n subchron, two within its older half (G2 and G3, Figures 6, 7, and 11) and a third micro-anomaly occurring just before the Gauss-Matuyama boundary (G1). It is of interest to mention that *Liddicoat et al.* [1980] found from a sedimentary section from the Searles Valley in California the same sequence of three short reversed polarity intervals during the C2An.1n subchron. The existence of a geomagnetic excursion slightly older than the Gauss-Matuyama boundary, which may be correlated with the microanomaly G1 from the CIR, is further supported by a recent magnetostratigraphic study of *Glen et al.* [1999a, 1999b], also from the Searles Valley, and by the occurrence of a pronounced paleointensity low during this period in the *Valet and Meynadier* [1993] record. The existence of the G1 event argues against the possibility suggested by *Westphal and Munschy* [1999] that the Gauss-Matuyama magnetic polarity reversal occurred over an unusually long duration.

7. Conclusion

We have investigated whether high-resolution magnetic oceanic profiles collected from the Central Indian Ridge provide a reliable high-resolution record of the geomagnetic field intensity. For the sake of comparison with paleointensity sequences obtained in sediments, the studied period was restricted to the last 3 Myr. A stacked deep-tow profile was constructed from six individual profiles obtained on both sides of the spreading axis. This stacked profile shows a dense succession of microanomalies within the Brunhes, the Matuyama, and the later part of the Gauss chrons. Stacked sea surface profiles constructed from the Central Indian Ridge, the East Pacific Rise, and the Pacific-Antarctic Ridge confirm the worldwide occurrence of most of these microanomalies and therefore indicate that they have a geomagnetic origin. For the Brunhes and the matuyama chrons, comparison of the CIR near bottom with paleointensity-derived synthetic profiles shows that the small-scale anomalies found in our data can be correlated with known low-paleointensity periods. The CIR results therefore indicate that field intensity variations are the main contributor to the shape of the recent marine magnetic anomalies in the CIR area.

Results inferred from the CIR near-bottom profiles suggest for the first time the occurrence of a relatively long-lasting magnetic anomaly slightly younger than the Olduvai subchron, which correlates with a succession of several geomagnetic events documented in sediments (Ontong Java 1 and 2 and Gilsa). The data also support the occurrence of three geomagnetic features (including the Réunion event) between the Gauss-Matuyama boundary and the Olduvai subchron. Our interpretation is less robust for the Gauss chron, for which the comparison between the deep-tow and

the synthetic profiles is quite unsatisfactory. If the stacked near-bottom profile for this period correctly reflects the geomagnetic field intensity fluctuations, three geomagnetic events would exist within the C2An.1n subchron.

Our study demonstrates the potential of deep-tow surveys for detecting the occurrence of short-lived geomagnetic events, although marine magnetic profiles cannot easily discriminate between subchrons and excursions. The analysis of near-bottom magnetic anomaly profiles could allow the establishment of the distribution of the short-lived geomagnetic events over the long period documented by the oceanic crust and for which magnetostratigraphic data are missing. This will be crucial to constrain the long-term behavior of the geomagnetic field, in particular for studying the link between magnetic reversal frequency and secular variation.

Acknowledgments. We thank Captain R. Gauthier and the crew of R/V *Marion Dufresne* for their efficient work during the Magofond 2 cruise; B. Ollivier and the IFRTP team for their help with data acquisition; and K. Tamaki and T. Sasaki, who kindly provided the deep-tow magnetometer. We are also grateful to P. Gente and R. Thibaud, who processed the bathymetric data; to H. Ondréas and L. Géli, who provided the PacAntarctique data; and to A. Briais and D. Sauter, who showed us helpful reflectivity data on the CIR. Thanks to M. Tivey for helping us with the deep-tow processing code. Finally, we thank S. Gilder, M. Cannat, J. Gee, R.C. Searle, and J.M. Hall for their helpful comments and suggestions during the manuscript writing. This is IPGP contribution 1734.

References

Allerton, S., J. Escartin, and S. Roger, Extremely asymmetric magmatic accretion of oceanic crust at the ends of slow-spreading ridge segments, *Geology*, *28*, 179-182, 2000.

Atwater, T., and J.D. Mudie, Detailed near-bottom geophysical study of the Gorda rise, *J. Geophys. Res.*, *78*, 8665-8686, 1973.

Baksi, A.K., K.A. Hoffman, and M. McWilliams, Testing the accuracy of the geomagnetic polarity time-scale [GPTS] at 2-5 Myr, utilizing $^{40}Ar/^{39}Ar$ incremental heating data on the whole-rock basalts, *Earth Planet. Sci. Lett.*, *118*, 135-144, 1993.

Ballard, R.D., and T.H. van Andel, Morphology and tectonics of the inner rift valley at lat. 36°50'N on the Mid-Atlantic Ridge, *Geol. Soc. Am. Bull.*, *88*, 507-530, 1977.

Blakely, R.J., Geomagnetic reversals and crustal spreading rates during the Miocene, *J. Geophys. Res.*, *79*, 2979-2985, 1974.

Blakely, R.J., and A. Cox, Evidence for short geomagnetic polarity intervals in the early Cenozoic, *J. Geophys. Res.*, *77*, 7065-7072, 1972.

Brown, J.R., and J.A. Karson,, Variations in axial processes in the Mid-Atlantic Ridge: The median valley of the MARK area, *Mar. Geophys. Res.*, *10*, 109-138, 1988.

Cande, S., and D.V. Kent, Constraints imposed by the shape of marine magnetic anomalies on the magnetic source, *J. Geophys. Res.*, *81*, 4157-4162, 1976.

Cande, S.C., and D.V. Kent, A new geomagnetic polarity time scale for the Late Cretaceous and Cenozoic, *J. Geophys. Res.*, *97*, 13,917-13,951, 1992a.

Cande S.C., and D.V. Kent, Ultrahigh resolution marine magnetic anomaly profiles: A record of continuous paleointensity variations, *J. Geophys. Res.*, *97*, 15,075-15,083, 1992b.

Cande, S., and D.V. Kent, Revised calibration of the geomagnetic polarity time scale, *J. Geophys. Res.*, *100*, 6093-6095, 1995.

Carlut, J., J.P. Valet, X. Quidelleur, V. Courtillot, T. Kidane, Y. Gallet, and P.Y. Gillot, Paleointensity across the Réunion event in Ethiopia, *Earth Planet. Sci. Lett.*, *170*, 17-34, 1999.

Champion, D.E., M.A. Lanphere, and M.A. Kuntz, Evidence for a new geomagnetic reversal from lava flows in Idaho: Discussion of short polarity reversals in the Brunhes and late Matuyama polarity chrons, *J. Geophys. Res.*, *93*, 11,667-11,680, 1988.

Chouckroune, P., J. Francheteau, and R. Hekinian, Tectonics of the East Pacific Rise near 12°50'N: A submersible study, *Earth Planet. Sci. Lett., 68*, 115-127,1984.

Clement, B.M., and D.V. Kent, Short polarity intervals within the Matuyama and transitional field records from hydraulic piston cored sediments from the North Atlantic, *Earth Planet. Sci. Lett.*, *81*, 253-264, 1987.

Cox, A., Geomagnetic reversals, *Science*, *163*, 237-245, 1969.

Dyment, J., and J. Arkani-Hamed, Spreading-rate dependent magnetization of the oceanic lithosphre inferred from the anomalous skewness of marine magnetic anomalies, *Geophys. J. Int.*, *121*, 789-804, 1995.

Dyment, J., et al., The magofond 2 cruise: A surface and deep-tow survey on the past and present CIR, *InterRidge News*, *8(1)*, 25-31, 1999a.

Dyment, J., A. Briais, Y. Gallet, and magofond-2 cruise scientific party, Morphology of the Central Indian Ridge near 19S: evidence for an influence of the R_union/Rodrigues hotspot, *EoS Trans AGU, 80*(46), Fall Meet. Suppl., F915, 1999b.

Emilia, D.A., and D.F. Heinrichs, Ocean floor spreading: Olduvai and Gilsa events in the Matuyama epoch, *Science*, *166*, 1267-1269, 1969.

Emilia, D.A., and D.F. Heinrichs, Paleomagnetic events in the Brunhes and Matuyama epochs identified from magnetic profiles reduced to the pole, *Mar. Geophys. Res.*, *1*, 436-444, 1972.

Fornari, D.J., R.M. Haymon, M.R. Perfit, and M.H. Edwards, Geological characteristics and evolution of the axial zone on fast spreading mid-ocean ridges: Formation of an axial summit trough along the East Pacific Rise, 9¡-10¡N, *J. Geophys. Res.*, *103*, 9827-9855, 1998.

Gallet, Y., J. Gee, L. Tauxe, and J. Tarduno, Paleomagnetic analysis of short normal polarity magnetic anomalies in the Matuyama chron, *Proc. Ocean Drill. Program Sci. Results, 130*, 547-559, 1993.

Gee, J., and D.V. Kent, Variations in layer 2A thickness and the origin of the central anomaly magnetic high, *Geophys. Res. Lett.*, *21*, 297-300, 1994.

Gee, J., D.A. Schneider, and D.V. Kent, marine magnetic anomalies as recorders of geomagnetic intensity variations, *Earth Planet. Sci. Lett., 144*, 327-335, 1996.

Géli, L., et al., Evolution of the Pacific-Antarctic Ridge south of the Udintsev Fracture Zone, *Science*, *278*, 1281-1284, 1997.

Gente, P., J.M. Auzende, V. Renard, Y. Fouquet, and D. Bideau, Detailed geological mapping by submersible of the East Pacific Rise axial graben near 13°N, *Earth Planet. Sci. Lett.*, *78*, 224-236, 1986.

Gente, P., C. Mével, J.M. Auzende, J.A. Karson, and Y., Fouquet, An example of a recent accretion on the Mid-Atlantic Ridge: the Snake Pit neovolcanic ridge (MARK area, 23°22'N), *Tectonophysics*, *190*, 1-29, 1991.

Glen, J., J.C. Liddicoat, and R.S. Coe, A long-term record of secular variation bounding the Gauss-Matuyama polarity reversal from Searles Lake, California, *EoS Trans AGU*, 80(46), Fall Meet. Suppl., F296, 1999a.

Glen, J. M. G., J.C. Liddicoat, and R.S. Coe, A detailed record of paleomagnetic field change from Searles Lake, California 2, The Gauss-Matuyama polarity reversal, *J. Geophys. Res.*, *104*, 12,883-12,894, 1999b.

Gubbins, D., The distinction between geomagnetic excursions and reversals, *Geophys. J. Int.*, *137*, F1-F3, 1999.

Guspi, F., Frequency-domain reduction of potential field measurements to a horizontal plane, *Geoexploration*, *24*, 87-98, 1987.

Guyodo, Y., and J.P. Valet, Relative variations in geomagnetic intensity from sedimentary records: The past 200 thousand years, *Earth Planet. Sci. Lett.*, *143*, 23-36, 1996.

Guyodo, Y., and J.P. Valet, Global changes in intensity of the Earth's magnetic field during the past 800 kyr, *Nature*, *399*, 249-252, 1999.

Guyodo, Y., C. Richter, and J.-P. Valet, Paleointensity record from Pleistocene sediments (1.4-0 Myr) off the California margin, *J. Geophys. Res.*, *104*, 22,953-22,964, 1999.

Harland, W.B., R.L. Amstrong, A.V. Cox, L.E. Craig, A.G. Smith, and D.G. Smith, *A Geologic Time Scale*, Cambridge Univ. Press, New York, 1989.

Heirtzler, J.R., G.O. Dickson, E.M. Herron, W.C. Pitman, III, and X.

Le Pichon,, Marine magnetic anomalies, geomagnetic field reversals, and motions of the ocean floor and continents, *J. Geophys. Res.*, *73*, 2119-2136, 1968.

Hussenoeder, S.A., M.A. Tivey, and H. Schouten, Direct inversion of potential fields from an uneven track with application to the Mid-Atlantic Ridge, *Geophys. Res. Lett., 22*, 3131-3134, 1995.

Hussenoeder, S.A., M.A. Tivey, H. Schouten, and R.C. Searle, Near bottom magnetic survey of the Mid-Atlantic Ridge axis, 24°-24°40'N: Implications for crustal accretion at slow spreading ridges, *J. Geophys. Res.*, *101*, 22,051-22,069, 1996.

International Association of Geomagnetism and Aeronomy (IAGA), Division V, Working Group 8, International geomagnetic reference field, 1995 revision, *Geophys. J. Int.*, *125*, 318-321, 1996.

Kidane, T., J. Carlut, V. Courtillot, Y. Gallet, X. Quidelleur, P.Y. Gillot, and T. Haile, Paleomagnetic and geochronological identification of the Réunion subchron in Ethiopian Afar, *J. Geophys. Res.*, *104*, 10,405-10,419, 1999.

Klitgord, K.D., Sea-floor spreading: The central anomaly magnetization high, *Earth Planet. Sci. Lett.*, *29*, 201-209, 1976.

Klitgord, K.D., S.P. Huestis, J.D. Mudie, and R.L. Parker, An analysis of near-bottom magnetic anomalies: Sea-floor spreading and the magnetized layer, *Geophys. J. R. Astron. Soc.*, *43*, 387-424, 1975

Kok, Y., and L. Tauxe, A relative paleointensity stack from Ontong-Java Plateau sediments for the matuyama, *J. Geophys. Res.*, *104*, 25,401-25,413, 1999.

LaBrecque, J.L., D.V. Kent, and S.C. Cande, Revised magnetic polarity time scale for Late Cretaceous and Cenozoic time, *Geology*, *5*, 330-335, 1977.

Lanci, L., and W. Lowrie, Magnetostratigraphic evidence that 'tiny wiggles' in the oceanic magnetic anomaly record represent geomagnetic paleointensity variations, *Earth Planet. Sci. Lett.*, *148*, 581-592, 1997.

Langereis, C.G., M.J. Dekkers, G.J. de Lange, M. Paterne, and P.J.M. van Santvoort, Magnetostratigraphy and astronomical calibration of the last 1.1 Myr from an eastern Mediterranean piston core and dating of short events in the Brunhes, *Geophys. J. Int.*, *129*, 75-94, 1997.

Lee, S.M., S.C. Solomon, and M. Tivey, Fine-scale crustal magnetization variations and segmentation of the East Pacific Rise, 9°10'-9°50'N, *J. Geophys. Res.*, *101*, 22,033-22,050, 1996.

Liddicoat, J.C., N.D. Opdyke, and G.I. Smith, Palaeomagnetic polarity in a 930-m core from Searles Valley, California, *Nature, 286*, 22-25, 1980.

Macdonald, K.C., Near-bottom magnetic anomalies, asymmetric spreading, oblique spreading, and tectonics of the Mid-Atlantic Ridge near lat 37°N, *Geol. Soc. Am. Bull.*, *88*, 621-636, 1977.

Macdonald, K.C., Mid-ocean ridges: Fine scale tectonic, volcanic and hydrothermal processes within the plate boundary zone, *Annu. Rev. Earth. Planet. Sci.*, *10*, 155-190, 1982.

Mankinen, E.A., and C.S. Gromme, Paleomagnetic data from the Coso range, California and current status of the Cobb Mountain Normal Geomagnetic Polarity Event, *Geophys. Res. Lett.*, *9*, 1279-1282, 1982.

Mankinen, E.A., J.M. Donnelly, and C.S. Grommé, Geomagnetic polarity event recorded at 1.1 m.y. B.P. on Cobb Mountain, Clear Lake volcanic field, California, *Geology*, *6*, 653-656, 1978.

McDougall, I., and N.D. Watkins, Age and duration of the Réunion geomagnetic polarity event, *Earth Planet Sci. Lett.*, *19*, 443-452, 1973.

Parker, R.L., The rapid calculation of potential anomalies, *Geophys. J. R. Astron. Soc.*, *31*, 447-455, 1973.

Parker, R.L., and S.P. Huestis, The inversion of magnetic anomalies in the presence of topography, *J. Geophys. Res.*, *79*, 1587-1593, 1974.

Perram, L.J., K.C. macdonald, and S.P. Miller, Deep-tow magnetics near 20°S on the East Pacific Rise: A study of short-wavelength anomalies at a very fast spreading center, *mar. Geophys. Res.*, *12*, 235-245, 1990.

Ravilly, M., J. Dyment, P. Gente, and R. Thibaud, Axial magnetic anomaly amplitude along the Mid-Atlantic Ridge between 20°N and 40°N, *Earth Planet. Sci. Lett.*, *103*, 24,201-24,221, 1998.

Rea, D.K., and R.J. Blakely, Short wavelength magnetic anomalies in a region of rapid sea-floor spreading, *Nature*, *255*, 126-128, 1975.

Sayanagi, K., A. Oshida, M. Watanabe, and K. Tamaki, New self-contained deep-towed proton magnetometer system, *J. Geomagn.Geoelectr.*, *46*, 631-662, 1994.

Schneider, D.A., and G.A. Mello, A high-resolution marine sedimentary record of geomagnetic intensity during the Brunhes Chron, *Earth Planet. Sci. Lett.*, *144*, 297-314, 1999.

Schouten, H., and C. Denham, Modeling the oceanic magnetic source layer, in *Deep Sea Drilling Results in the Atlantic Ocean: Ocean Crust Maurice Ewing Ser.*, vol. 2, edited by M. Talwani, C.G.A. Harrison and D.E. Hayes, pp. 151-159, AGU, Washington, DC, 1979.

Schouten, H., and K. McCamy, filtering marine magnetic anomalies, *J. Geophys. Res.*, *77*, 7089-7099, 1972.

Schouten, H., M. A. Tivey, D. Fornari, and J.R. Cochran, Central anomaly magnetization high: Constraints on the volcanic construction and architecture of seismic layer 2A at a fast-spreading mid-ocean ridge, the EPR at 9°30'-50'N, *Earth Planet. Sci. Lett.*, *169*, 37-50, 1999.

Shuey, R.T., and F.H. Brown, magnetostratigraphy of the Shungura formation, southwestern Ethiopia: Fine structure of the lower Matuyama polarity epoch, *Earth Planet. Sci. Lett.*, *23*, 249-260, 1974.

Singer, B., K. Hoffman, A. Chauvin, R. Coe, and M. Pringle, Dating transitionally magnetized lavas of the late matuyama chron: Toward a new $^{40}Ar/^{39}Ar$ timescale of reversals and events, *J. Geophys. Res.*, *104*, 679-693, 1998.

Smith, D.K., and J.R. Cann, Constructing the upper crust of the Mid-Atlantic Ridge: A reinterpretation based on the Puna Ridge, Kilauea Volcano, *J. Geophys. Res.*, *104*, 25,379-25,399, 1999.

Smith, D.K., M.A. Tivey, H. Schouten, and J.R. Cann, Locating the spreading axis along 80 km of the Mid-Atlantic Ridge south of the Atlantis Transform, *J. Geophys. Res.*, *104*, 7599-7612, 1999.

Tisseau, J., and P. Patriat, Identification des anomalies magnétiques sur les dorsales à faible taux d'expansion: Méthode des taux fictifs, *Earth Planet. Sci. Lett.*, *52*, 381-396, 1981.

Tivey, M.A., and H.P. Johnson, The central anomaly magnetic high: Implications for ocean crust construction and evolution, *J. Geophys. Res.*, *92*, 12,685-12,694, 1987.

Tivey, M.A., and H.P. Johnson, Variations in oceanic crustal structure and implications for the fine-scale magnetic anomaly signal, *Geophys. Res. Lett.*, *20*, 1879-1882, 1993.

Valet, J.P., and L. Meynadier, Geomagnetic field intensity and reversals during the past four million years, *Nature*, *366*, 234-238, 1993.

Westphal, M., and M. Munschy, Un test de la variation en dents de scie du champ magnétique terrestre par les anomalies du champ magnétique sur les dorsales, *C. R. Acad. Sci., Ser.* II*a*, *329*, 565-571, 1999.

Wilson, D.S., and R.N. Hey, The Galapagos axial magnetic anomaly: Evidence for the Emperor event within the Brunhes and for a two-layer magnetic source, *Geophys. Res. Lett.*, *10*, 1051-1054, 1981.

J. Dyment, UMR 6538, IUEM, Université de Bretagne Occidentale, 1 Place N Copernic, F-29280 Plouzané, France. (jerome@univ-brest.fr)

Y. Gallet, IPGP, Laboratoire de Paléomagnétisme, Tour 24-14, 1er etage, 4 place Jussieu, F-75252 Paris Cedex 05, France. (gallet@ipgp.jussieu.fr)

P. Patriat, and G. Pouliquen, IPGP, Laboratoire de Gravimétrie et Géodynamique, Tour 26-0, 1er etage, 4 place Jussieu, F-75252 Paris Cedex 05, France. (poulique@ipgp.jussieu.fr)

C. Tamura, Ocean Research Institute, University of Tokyo, Tokyo, Japan. (chiori@ori.u-tokyo.ac.jp)

(Received June 20, 2000; revised October 30, 2000; accepted November 28, 2000.)